TURUN
YLIOPISTO
UNIVERSITY
OF TURKU

QUANTITATIVE MAGNETIC RESONANCE IMAGING AND HIGH-INTENSITY FOCUSED ULTRASOUND TREATMENT OF UTERINE FIBROIDS

Teija Sainio

TURUN YLIOPISTON JULKAISUJA – ANNALES UNIVERSITATIS TURKUENSIS
SARJA – SER. D OSA – TOM. 1593 | MEDICA – ODONTOLOGICA | TURKU 2021

TURUN
YLIOPISTO
UNIVERSITY
OF TURKU

QUANTITATIVE MAGNETIC RESONANCE IMAGING AND HIGH-INTENSITY FOCUSED ULTRASOUND TREATMENT OF UTERINE FIBROIDS

Teija Sainio

TURUN YLIOPISTON JULKAISUJA – ANNALES UNIVERSITATIS TURKUENSIS
SARJA – SER. D OSA – TOM. 1593 | MEDICA – ODONTOLOGICA | TURKU 2021

University of Turku

Faculty of Medicine
Medical Physics and Engineering
Doctoral Programme in Clinical Research
Department of Medical Physics, Turku University Hospital
Department of Radiology, Turku University Hospital

Supervised by

Professor Roberto Blanco Sequeiros
Department of Clinical Medicine
University of Turku
Turku, Finland

Docent Jani Saunavaara
Department of Clinical Medicine
University of Turku
Turku, Finland

Reviewed by

Associate Professor Mikko Nissi
Department of Applied Physics
University of Eastern Finland
Kuopio, Finland

Professor Seppo Koskinen
Department of Clinical Science
Karolinska Institutet
Stockholm, Sweden

Opponent

Professor Kullervo Hynynen
Department of Medical Biophysics
University of Toronto
Toronto, Canada

The originality of this publication has been checked in accordance with the University of Turku quality assurance system using the Turnitin OriginalityCheck service.

ISBN 978-951-29-8692-7 (PRINT)
ISBN 978-951-29-8693-4 (PDF)
ISSN 0355-9483 (Print)
ISSN 2343-3213 (Online)
Painosalama, Turku, Finland 2021

"The important thing is not to stop questioning. Curiosity has its own reason for existence. One cannot help but be in awe when he contemplates the mysteries of eternity, of life, of the marvelous structure of reality. It is enough if one tries merely to comprehend a little of this mystery each day. "

Albert Einstein

UNIVERSITY OF TURKU
Faculty of Medicine
Department of Clinical Medicine
Medical Physics and Engineering
TEIJA SAINIO: Quantitative magnetic resonance imaging and high-intensity focused ultrasound treatment of uterine fibroids.
Doctoral Dissertation, 100 pp.
Doctoral Programme in Clinical Research
November 2021

ABSTRACT

Magnetic resonance-guided high-intensity focused ultrasound (MRgHIFU) treatment is an emerging non-invasive treatment method in which the targeted tissue is heated by high-intensity ultrasound causing coagulative necrosis. Benign muscle tumors of the uterus alias uterine fibroids can be treated with MRgHIFU though treatment outcomes have been varying. Treatment outcomes are affected by different properties of uterine fibroid tissue such as blood flow and histological structure. The blood flow of uterine fibroids can be changed by oxytocin infusion even though oxytocin's mechanism of action on the blood flow of uterine fibroids is unknown.

The present magnetic resonance imaging (MRI) based evaluation methods of uterine fibroids' suitability for MRgHIFU treatment are not completely satisfactory. Quantitative MRI techniques can be used for measuring the histological properties of tissues in an indirect manner, which could be better for uterine fibroids' suitability evaluation. This study investigated the feasibility of applying quantitative MRI techniques; diffusion-weighted imaging (DWI) and T2 relaxation time mapping, to predict outcomes of the MRgHIFU treatment of uterine fibroids. Based on these results, new quantitative evaluation methods were developed and compared with currently used MRI-based evaluation methods. In addition, the effect of oxytocin on the blood flow of the uterine fibroid and the myometrium was studied quantitatively using dynamic contrast-enhanced magnetic resonance imaging (DCE-MRI).

The results of this study indicate that DWI and T2 relaxation time mapping are feasible for the evaluation of MRgHIFU treatment outcomes. Evaluation methods based on these techniques also appear to be more reliable than current approaches. When utilizing DCE-MRI, it was observed that oxytocin strongly reduced the blood flow of uterine fibroids without affecting the blood flow in the myometrium, indicating that oxytocin's effect took place solely in the uterine fibroid. The results of this work are directly applicable to the clinical practice of treating uterine fibroids with MRgHIFU.

KEYWORDS: uterine fibroid, high-intensity focused ultrasound, magnetic resonance imaging, diffusion-weighted imaging, T2 relaxation time mapping, dynamic contrast-enhanced imaging

TURUN YLIOPISTO
Lääketieteellinen tiedekunta
Kliininen laitos
Lääketieteellinen fysiikka ja tekniikka
TEIJA SAINIO: Myoomien kvantitatiivinen magneettikuvantaminen ja korkea intensiteettinen fokusoitu ultraäänihoito.
Väitöskirja, 100 s.
Turun kliininen tohtoriohjelma
Marraskuu 2021

TIIVISTELMÄ

Magneettikuvausohjattu korkeaintensiteettinen kohdennettu ultraäänihoito (magnetic resonance-guided high-intensity focused ultrasound, MRgHIFU) on uudenlainen kajoamaton hoitomenetelmä, jossa kohdekudosta lämmitetään korkeaintensiteettisen ultraäänen avulla, mikä aiheuttaa koagulaationekroosia. Kohdun hyvänlaatuisia lihaskasvaimia eli myoomia voidaan hoitaa MRgHIFU-hoidolla, mutta hoitotulokset ovat kuitenkin vaihtelevia. Hoitotuloksiin vaikuttavat myoomakudoksen erilaiset ominaisuudet kuten verenvirtaus ja histologinen rakenne. Myoomien verenvirtausta voidaan muuttaa oksitosiini-infuusiolla, mutta oksitosiinin vaikutusmekanismi myoomien verenvirtaukseen ei ole tunnettu.

Nykyiset magneettikuvaukseen perustuvat myoomien soveltuvuuden arviointimenetelmät MRgHIFU-hoitoon eivät ole täysin tyydyttäviä. Kvantitatiivisilla magneettikuvaustekniikoilla voidaan mitata epäsuorasti kudosten histologisia ominaisuuksia ja siten nämä tekniikat voisivat olla parempia myoomien soveltuvuuden arvioinnissa MRgHIFU-hoitoon. Tässä tutkimuksessa arvioitiin kvantitatiivisten magneettikuvaustekniikoiden (diffuusiopainotettu kuvantaminen ja T2-relaksaatioaikakartoitus) soveltuvuutta ennustaa myoomien MRgHIFU-hoitotuloksia. Näiden tulosten perusteella kehitettiin uudet kvantitatiiviset arviointimenetelmät ja verrattiin näitä menetelmiä nykyisiin magneettikuvaukseen perustuviin arviointimenetelmiin. Lisäksi oksitosiinin vaikutusta myooman ja kohdun seinämän verenvirtaukseen tutkittiin kvantitatiivisesti käyttäen dynaamista kontrastiainetehosteista magneettikuvantamista.

Tutkimuksen tulokset osoittivat, että diffuusiopainotettu kuvantaminen ja T2-relaksaatioaikakartoitus soveltuvat myoomien MRgHIFU-hoitotulosten arviointiin. Näihin tekniikoihin perustuvat arviointimenetelmät vaikuttavat olevan myös luotettavampia kuin nykyiset arviointimenetelmät. Dynaamisen kontrastitehosteisen magneettikuvantamisen avulla havaittiin, että oksitosiini vähentää voimakkaasti myooman verenvirtausta vaikuttamatta kohdun seinämän verenvirtaukseen viitaten siihen, että oksitosiinin vaikutus tapahtuu vain myoomassa. Tämän työn tulokset ovat suoraan sovellettavissa myoomien MRgHIFU-hoitojen kliinisiin käytäntöihin.

AVAINSANAT: myooma, korkeaintensiteettinen kohdennettu ultraääni, magneettikuvaus, diffuusiopainotettu kuvantaminen, T2-relaksaatioaikakartoitus, dynaaminen kontrastitehosteinen kuvantaminen

Table of Contents

Abbreviations

ADC	Apparent diffusion coefficient
AIF	Arterial input function
BF	Blood flow
CA	Contrast agent
CPMG	Carr-Purcell-Meiboom-Gill
CE	Contrast-enhanced
CEM43	Cumulative equivalent minutes at 43°C
DCE-MRI	Dynamic contrast-enhanced magnetic resonance imaging
DWI	Diffusion-weighted imaging
ECM	Extracellular matrix
EPI	Echo planar imaging
FIGO	The International Federation of Gynecology and Obstetrics
GRASE	Gradient echo and spin echo
GRE	Gradient echo
HIFU	High-intensity focused ultrasound
IR	Inversion recovery
MRgHIFU	Magnetic resonance-guided high-intensity focused ultrasound
MRI	Magnetic resonance imaging
NPV	Non-perfused volume
NPVr	Non-perfused volume ratio
PRF	Proton resonance frequency
QMRI	Quantitative magnetic resonance imaging
RF	Radiofrequency
RLSQ	Ratios and least squares
ROC	Receiver-operating-characteristic
ROI	Region of interest
rT2	Relative T2 signal intensity
SE	Spin echo
SSI	Scaled signal intensity
TE	Echo time
TI	Inversion time

TR	Repetition time
TSE	Turbo spin echo
T1W	T1-weighted
T2W	T2-weighted
UAE	Uterine artery embolization
US	Ultrasound
USgHIFU	Ultrasound-guided high-intensity focused ultrasound
VFA	Variable flip angle
2CM	Two-compartment exchange model

List of Original Publications

This dissertation is based on the following original publications, which are referred to in the text by their Roman numerals I-III:

I Otonkoski S*, Sainio T*, Komar G, Suomi V, Saunavaara J, Blanco Sequeiros R, Perheentupa A, Joronen K. Oxytocin selectively reduces blood flow in uterine fibroids without an effect on myometrial blood flow: a dynamic contrast enhanced MRI evaluation. International Journal of Hyperthermia. 2020;37(1):1293-1300.

II Sainio T, Saunavaara J, Komar G, Mattila S, Otonkoski S, Joronen K, Perheentupa A, Blanco Sequeiros R. Feasibility of apparent diffusion coefficient in predicting the technical outcome of MR-guided high-intensity focused ultrasound treatment of uterine fibroids - a comparison with the Funaki classification. International Journal of Hyperthermia. 2021;38(1):85-94.

III Sainio T, Saunavaara J, Komar G, Otonkoski S, Joronen K, Viitala A, Perheentupa A, Blanco Sequeiros R. Feasibility of T2 relaxation time in predicting the technical outcome of MR-guided high-intensity focused ultrasound treatment of uterine fibroids. International Journal of Hyperthermia. 2021;38(1):1384-1393.

*These authors contributed equally to this work.

1 Introduction

Benign uterine smooth-muscle cell tumors also known as uterine fibroids (leiomyomas or myomas) are the most common tumors encountered in women affecting up to two out of every three women of premenopausal age (Cramer & Patel, 1990; Stewart, 2001). Up to 30% of fibroid cases may cause severe symptoms which can include abnormal uterine bleeding, pelvic pressure and pain, and reproductive dysfunction (Donnez & Dolmans, 2016; Havryliuk et al., 2017). Symptomatic uterine fibroids can be treated with medical therapy, surgery, uterine artery embolization (UAE), and imaging-guided high-intensity focused ultrasound (HIFU) (Parker, 2007).

Magnetic resonance-guided high-intensity focused ultrasound (MRgHIFU) treatment is an emerging non-invasive treatment method that is based on the heating capability of high-intensity ultrasound that can evoke coagulative necrosis of the targeted tissue which is combined with real-time magnetic resonance imaging (MRI) to ensure temperature mapping and anatomical monitoring during the treatment (Jolesz, 2009). MRgHIFU treatment has been shown to be a safe and effective treatment method for symptomatic uterine fibroids (Funaki et al., 2009; Stewart et al., 2007; Tempany et al., 2003). However, the extensive histological heterogeneity has been observed within and between uterine fibroids which can cause suboptimal MRgHIFU treatment results (Funaki et al., 2007; Holdsworth-Carson et al., 2016; Jayes et al., 2019; Magalhães Peregrino et al., 2017;Wei et al., 2006). To achieve the most optimal treatment result, careful screening and selection of patients before MRgHIFU treatment of uterine fibroids is usually performed using MRI (Duc & Keserci, 2018; Sridhar & Kohi, 2018).

The most commonly used selection methods are based on relative signal intensities in T2-weighted (T2W) images; the Funaki classification and scaled signal intensity (SSI) method (Funaki et al., 2007; Park et al., 2015). However, T2W imaging is a qualitative method in which signal intensity and image contrast are influenced by several factors, e.g., the coil receiver sensitivity, gain effects, and imaging parameters (Bojorquez et al., 2017; Hardy et al., 1992). On the other hand, quantitative MRI methods are largely independent of these factors and could therefore provide a more reliable and comparable assessment of tissue histology and

a better prediction of the technical treatment outcome. Previous studies have shown that quantitative texture and perfusion parameters correlate with ablation efficiency, heating efficiency, and/or non-perfused volume ratio (NPVr) (Hocquelet et al., 2017; Kim et al., 2011; Kim, et al., 2012, 2014;Wei et al., 2017).

In addition to the careful selection of patients before treatment, the MRgHIFU treatment efficacy has been shown to improve with intravenous oxytocin infusion (Lozinski et al., 2018). The improvement of the efficacy could be due to the reduction of the blood flow related factors of the uterine fibroids (Wang et al., 2016). However, the mechanism behind this phenomenon has not been thoroughly investigated. A quantitative perfusion MRI method could provide a more reliable assessment of blood flow changes evoked by oxytocin infusion in different types of uterine fibroids and the surrounding tissues, and also help to clarify the effects of oxytocin on the tissue level.

The present work aimed to assess the feasibility of quantitative MRI techniques (diffusion-weighted imaging, T2 relaxation time mapping) in predicting the technical outcome of MRgHIFU treatment of uterine fibroids and to compare these new quantitative MRI evaluation methods to the currently most commonly utilized methods. For this purpose, a multiparametric MRI was performed before MRgHIFU treatment and the technical outcomes of MRgHIFU treatments were defined. In addition, the effects of oxytocin infusion on the blood flow of uterine fibroids and surrounding tissues were evaluated with a quantitative MRI technique (dynamic contrast-enhanced magnetic resonance imaging) by performing two MRI scans without and with oxytocin infusion during the MRI scan in healthy volunteers and patients presenting with uterine fibroids.

2 Review of the Literature

2.1 Uterine fibroids

Uterine fibroids (also known as leiomyomas and myomas) are benign uterine tumors which arise from the myometrium (Donnez & Dolmans, 2016; Stewart, 2001). In histological terms, uterine fibroids consist of smooth muscle cells and myofibroblasts which produce extracellular matrix (ECM) containing collagen, fibronectin, and proteoglycans (Donnez & Dolmans, 2016; Parker, 2007). Uterine fibroids can cause symptoms such as abnormal uterine bleeding, pelvic pressure and pain, and reproductive dysfunction which can depend on the location, quantity, and size of the uterine fibroid(s) (Havryliuk et al., 2017; Stewart, 2001). Uterine fibroids can be in several possible locations e.g. in the submucosa (submucosal), within the myometrium (intramural), outside the myometrium (subserosal), and pedunculated(Stewart, 2001). However, uterine fibroids can be present in multiple locations at the same time. The International Federation of Gynecology and Obstetrics (FIGO) created a uterine fibroid classification that describes eight types of uterine fibroids, denoted as types 0-8 (Figure 1) (Munro et al., 2011).

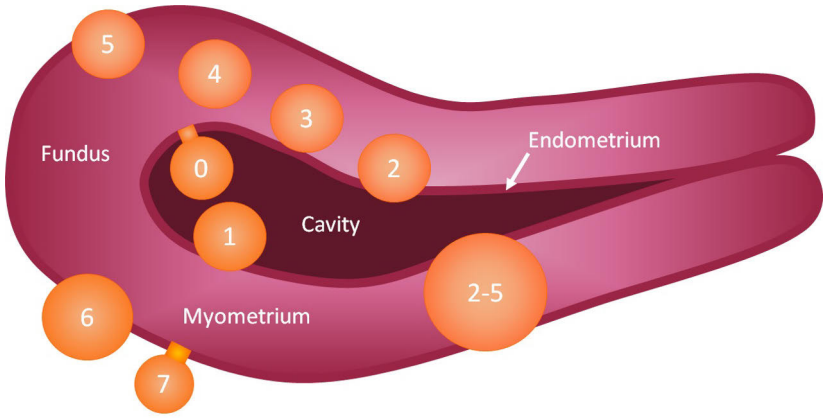

Figure 1. The FIGO classification of uterine fibroids where types range from 0-8; 0 = submucosal pedunculated intracavitary; 1 = submucosal, < 50% intramural; 2 = submucosal, ≥ 50% intramural; 3 = 100% intramural and endometrial contact, 4 = 100% intramural; 5 = subserosal and ≥ 50% intramural; 6 = subserosal and < 50% intramural; 7 = subserosal pedunculated; 8 = other; and 2-5 = submucosal, subserosal and ≥ 50% intramural.

Symptomatic uterine fibroids can be treated with medical therapy, hysterectomy, myomectomy, and minimally invasive techniques such as uterine artery embolization (UAE) and imaging-guided high-intensity focused ultrasound (HIFU) (Khan et al., 2014; Parker, 2007). Hysterectomy is the only definitive treatment for uterine fibroids but minimally invasive treatment methods offer many advantages in comparison with hysterectomy such as lower morbidity, shorter recovery time, and sparing of uterus and fertility (Khan et al., 2014; Mindjuk et al., 2014). In addition, magnetic resonance-guided high-intensity focused ultrasound (MRgHIFU) can be more cost-effective when compared with UAE, hysterectomy, and myomectomy (Zowall et al., 2008). In Turku University Hospital, the MRgHIFU treatment of uterine fibroid(s) costs about 2300 euros, which is similar when compared to hysterectomy (2400 euros), myomectomy (2100 euros), and UAE (1370 euros) without taking into account the hospital stays.

2.2 High-intensity focused ultrasound (HIFU)

Sound is a mechanical disturbance of an equilibrium state which propagates through the medium. Sound can be divided according to the frequency such that sound waves below 20 Hz are known as infrasound and those above 20 kHz are known as ultrasound both being inaudible to the human ear. The frequency of the ultrasound that has been used in the diagnostics varies in a range of 1 to 20 MHz. (Samei et al., 2019)

When an ultrasound wave propagates through tissue, the total loss (attenuation) of ultrasound energy is caused by scattering, absorption, refraction, and reflection (Hill et al., 2004). The absorption of the ultrasound causes an elevation in the tissue temperature which is proportional to the local intensity of the ultrasound (Hill et al., 2004; Samei et al., 2019). Tissues have specific attenuation coefficients due to their different tissue properties e.g. attenuation coefficients of skeletal blood plasma, skeletal muscle, and bone at 1 MHz are 0.28 dB/cm, 0.74 dB/cm, and 20.0 dB/cm, respectively (Samei et al., 2019).

High-intensity focused ultrasound (HIFU) is generated by focusing ultrasound waves in a small well-defined volume which creates a high-intensity focus into targeted tissue (ter Haar, 1999; ter Haar & Coussios, 2007). Ultrasound waves can be focused by using a spherically curved phased array ultrasound transducer which consists of multiple transducer elements (ter Haar, 1999; ter Haar & Coussios, 2007). A schematic illustration of a HIFU setup is presented in Figure 2. The high-intensity of ultrasound in the focus can cause a rapid rise in temperature which can induce coagulative necrosis of the targeted tissue while leaving the surrounding tissues intact (ter Haar & Coussios, 2007).

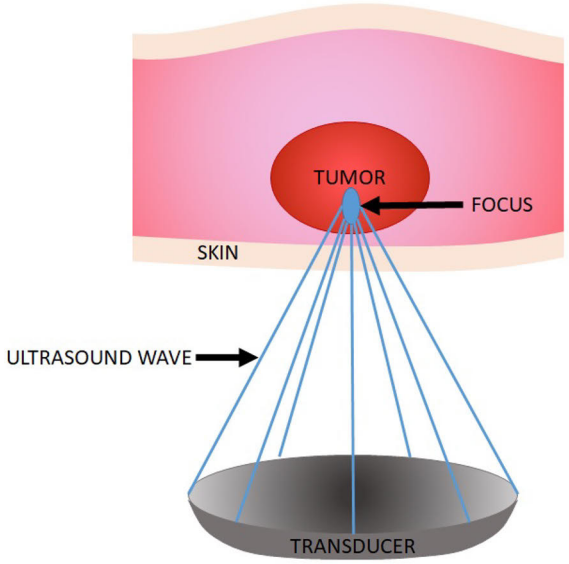

Figure 2. An illustration of ultrasound waves focused by a spherical HIFU transducer propagating through skin and intervening tissue to the targeted tumor tissue.

2.2.1 Thermal ablation

Thermal ablation is the local application of extremely elevated tissue temperatures (hyperthermia) or depressed tissue temperatures (hypothermia), which can induce an irreversible cell injury and ultimately tissue apoptosis and coagulative necrosis (Brace, 2011; Chu & Dupuy, 2014).

The biological effect of temperature rise depends on the temperature and the heating duration (Damianou et al., 1995). Thermal dose of any temperature profile can be calculated by using a method proposed by Sapareto and Dewey (Sapareto & Dewey, 1984). The method uses numerical integration to calculate equivalent minutes which correspond to the thermal dose at a reference temperature which is usually defined as 43 degrees of Celsius (Sapareto & Dewey, 1984). The relationship between thermal dose and temperature profile is defined as follows:

$$\boldsymbol{TD_{43}(t) = \int_0^t R^{43\,^{\circ}\mathrm{C}-\mathrm{T}(t)}\, dt} \qquad (1)$$

where TD_{43} is thermal dose in equivalent minutes, i.e., cumulative equivalent minutes at reference temperature of 43 °C (CEM43), t duration of exposure in minutes, T is the temperature, and R is a constant which depends on the temperature (R= 0.25, T < 43 °C and R= 0.5, $T \geq$ 43 °C) (Sapareto & Dewey, 1984). The threshold of the thermal dose for necrosis has been shown to be 30-250 CEM43 depending on the tissue type e.g. the threshold thermal dose for muscle tissue is between 120-240

CEM43 (Damianou et al., 1995; Damianou & Hynynen, 1994). Usually, 240 CEM43 has been used as a general threshold of the thermal dose for all soft tissue types as it has been shown to evoke a total necrosis in most tissue types (McDannold et al., 2000; Venkatesan et al., 2012).

2.2.2 Imaging-guided HIFU

Imaging guidance refers to procedures in which imaging techniques, such as ultrasound, fluoroscopy, and magnetic resonance imaging, are used during the procedure (Goldberg et al., 2005). In the procedure, imaging is used for planning, targeting, monitoring, controlling, and assessing the treatment response (Goldberg et al., 2005). The HIFU treatment can be guided with ultrasound (US) or magnetic resonance imaging (MRI) (Jenne et al., 2012; She et al., 2016; ter Haar & Coussios, 2007).

Ultrasound imaging is the most widespread method for the guidance of HIFU treatment (USgHIFU) (Jenne et al., 2012). USgHIFU is cost-effective because the therapeutic and imaging ultrasound transducers can be integrated into the same system, nonetheless, ultrasound imaging has a relatively low spatial resolution which limits the targeting accuracy of the HIFU treatment (Jolesz, 2009; She et al., 2016). In USgHIFU treatment, the tissue ablation cannot be monitored with US thermometry due to the inadequate accuracy above 50 °C, which is caused by non-linear temperature dependencies of contrast parameters, tissue phase-transitions, and cavitation bubbles (Raiko et al., 2020). Tissue ablation is usually monitored using a visual assessment of hyperechoic (bright) regions on the ultrasound image (Jenne et al., 2012; Rivens et al., 2009). In addition, USgHIFU does not require patient to be in enclosed space and ultrasound imaging is quiet which improves patient comfort (Zhang et al., 2015).

On the other hand, MRI offers excellent spatial resolution and sensitive real-time thermometry for the guidance of the HIFU treatment (Jenne et al., 2012; Jolesz, 2009; She et al., 2016). The real-time thermometry allows the detection of thermal changes before any irreversible tissue damage occurs and the calculation of accumulated thermal dose which predicts the extent of the tissue damage (Jenne et al., 2012; She et al., 2016). MR thermometry is based on temperature-sensitive MR parameters of which the most commonly used is the proton resonance frequency (PRF) due to its excellent linearity of temperature dependency (De Senneville et al., 2005; Rieke & Pauly, 2008). However, MRI guidance is expensive and scanner noise can be disturbing for patient when compared to ultrasound imaging (Jenne et al., 2012; She et al., 2016). The MRI limits also the patient selection for the HIFU treatment due to the possible MRI incompatible implants or foreign objects, or claustrophobia (Rueff & Raman, 2013; Sammet, 2016).

2.2.3 MRgHIFU treatment of uterine fibroids

Usually, the MRgHIFU treatment procedure of uterine fibroids consists of five phases: screening, preparation, planning, therapy, and outcome assessment (Sridhar & Kohi, 2018).

Screening

Generally, patient screening prior to the MRgHIFU treatment includes a clinical assessment and an MRI examination in which anatomical and MRI properties of uterine fibroids and adjacent tissues are assessed (Hesley et al., 2013; Keserci & Duc, 2018). The clinical assessment may consist of a patient interview (e.g. symptoms and prior treatments) and physical examination (Rueff & Raman, 2013).

From the MR images, uterine position, fibroid location, fibroid size, number of fibroids, abdominal scars, the thickness of abdominal subcutaneous fat, and distance between skin and fibroid(s) are assessed (Duc & Keserci, 2018; Hesley et al., 2008, 2013;Kim et al., 2014;Park et al., 2015; Yoon et al., 2008; Zaher et al., 2009). There are many reasons why a patient is assessed as being unsuitable for MRgHIFU treatment: 1) patients with a retroverted uterus (transducer target distance), 2) pedunculated subserosal fibroid (risk of unattachement), 3) fibroid diameter larger than 10 cm (cannot be treated in one session) or smaller than 2-3 cm (adjacenting tissues restrict beam path), 4) five or more symptomatic fibroids (treatment efficacy decreases), 5) extensive abdominal scarring which cannot be covered with an acoustic patch (skin burn due to attenuation), 6) excessively thick abdominal subcutaneous fat (increased attenuation), 7) the distance between the skin and fibroids is over 10 cm (Sonalleve system) or 12 cm (ExAblate system) (transducer focus distance), or 8) critical obstacles such as bowels or ovaries in the ultrasound beam path that cannot be shifted or avoided (complication risk) (Duc & Keserci, 2018; Hesley et al., 2008, 2013;Kim et al., 2014;Park et al., 2015; Yoon et al., 2008; Zaher et al., 2009).

The characteristics of uterine fibroid(s) in respect of adjacent tissues are defined via the T1 and/or T2 signal intensities which are used for assessing the suitability of uterine fibroids and predicting treatment outcome (Funaki et al., 2007; Mindjuk et al., 2014;Park et al., 2015).

The signal intensity of the uterine fibroid relative to the myometrium on fat-saturated T1-weighted (T1W) contrast-enhanced (CE) images enables classification into four types: CE-type 1 (hypointense); CE-type 2 (hypo- to isointense); CE-type 3 (isointense); and CE-type 4 (hyperintense) (Mindjuk et al., 2014). Based on a previous study, CE-type 4 fibroids are usually not suitable for MRgHIFU treatment probably due to higher perfusion (Mindjuk et al., 2014).

The Funaki classification is based on signal intensities of uterine fibroid, abdominal muscle, and myometrium on T2W MR images in which uterine fibroids are classified into three types: Funaki type I, hypointense (comparable to that of skeletal muscle); Funaki type II, intermediate (lower than that of the myometrium but higher than that of the skeletal muscle); and Funaki type III, hyperintense (equal to or higher than that of the myometrium) which are presented in Figure 3 (Funaki et al., 2007). In the screening, usually type I and type II fibroids are considered as most suitable for the MRgHIFU treatment, whereas type III fibroids are not amenable (Funaki et al., 2007). High signal intensity in T2W images has been correlated with high proliferative activity and high cellularity, which could explain poor treatment outcomes in Funaki type III fibroids (Oguchi et al., 1995; Swe et al., 1992). The imaging parameters of T2W sequence have been shown to influence in the Funaki classification and therefore, special attention should be paid in the imaging parameters of the screening T2W sequence (Verpalen et al., 2020).

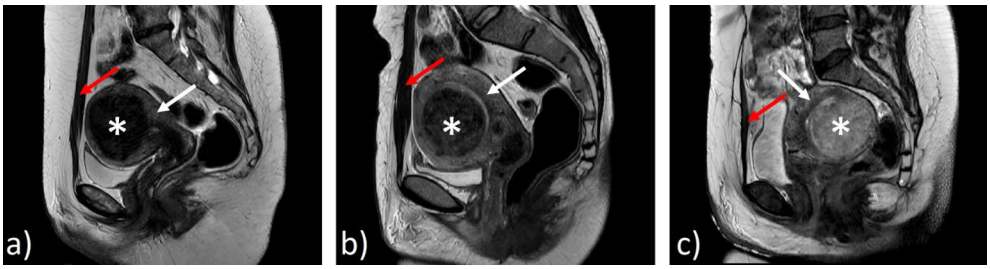

Figure 3. A presentation of different Funaki type uterine fibroid appearances in sagittal T2-weighted MR images: a) Funaki type I (hypointense), b) Funaki type II (intermediate), and c) Funaki type III (hyperintense) where structures uterine fibroid, myometrium, and skeletal muscle are denoted with asterisk, white arrow and red arrow, respectively. The imaging parameters were a) TE= 95 ms, TR=4844 ms, slice thickness=3mm, and field of view=240x240 mm.

The scaled signal intensity (SSI) classification is a relatively new T2W-based classification in which the signal intensity of uterine fibroid is compared to the signal intensity of the abdominal muscle and abdominal fat on a scale of 0-100 (H. Park et al., 2015). The SSI can be calculated according to Equation 2 (H. Park et al., 2015).

$$\mathbf{SSI} = \frac{\boldsymbol{SI\ of\ the\ uterine\ fibroid - SI\ of\ the\ abdominal\ muscle}}{\boldsymbol{SI\ of\ the\ abdominal\ fat - SI\ of\ the\ abdominal\ muscle}} \quad (2)$$

Based on the previous study uterine fibroids with an SSI value less than 16.0 are expected to be suitable for the MRgHIFU treatment (Park et al., 2015).

In addition, several other MRI-related factors have been shown to predict the technical treatment outcome or the treatment efficiency parameters of the MRgHIFU

of uterine fibroid therapy for example fibroid perfusion parameters, and texture parameters (Hocquelet et al., 2017; Kim et al., 2011, 2012, 2016; Li et al., 2020; Wei et al., 2017).

Patient preparation

Patient preparation for the MRgHIFU treatment of the uterine fibroids usually consists of overnight fasting, depilation of the lower abdomen, insertion of the an intravenous line for moderate sedation and possible oxytocin infusion during the treatment, Foley catheter insertion for bladder manipulation during the treatment, and assessment by the treating physician (Hesley et al., 2008, 2013;Kim et al., 2016; Lozinski et al., 2018; Zhu et al., 2016). Patient monitoring for blood pressure, heart rate, and oxygenation can also be undertaken during the MRgHIFU treatment (Hesley et al., 2008; Lozinski et al., 2018). The patient is positioned on the HIFU table in a prone position and acoustic coupling between the skin and the device can be achieved with deionized and degassed water (Hesley et al., 2008, 2013; Sainio et al., 2018). The acoustic coupling can be confirmed by acquiring gradient-echo T1W images where air bubbles in the ultrasound beam path can be detected (Sainio et al., 2018).

Planning

The planning of MRgHIFU treatment is performed immediately before the treatment and a multiplane or a 3D T2W image is acquired to assure proper positioning of uterine fibroid(s) and a safe ultrasound beam path to the uterine fibroid(s) (Hesley et al., 2008, 2013; Rueff & Raman, 2013; Sainio et al., 2018; Zhu et al., 2016). The T2W images are used to define the target volume and to place the therapy cells on the images by taking into account safety margins from critical organs such as the bowel and ovaries (Keserci & Duc, 2018; Liu et al., 2014; Zhu et al., 2016). The therapy cell (see Figure 4) is an ellipsoidal volume of 0.08, 0.67, 2.26, 3.59, and 5.36 mL, corresponding to axial diameter of 4, 8, 12, 14, or 16 mm (Sonalleve system), respectively (Zhu et al., 2016).

Treatment

The MRgHIFU treatment is delivered as a series of individually focused ultrasound pulses also known as sonications (Hesley et al., 2013). At the beginning of the treatment, therapy sonication power (e.g. 140-300 W) is determined by the heat response from a test sonication which is performed with low power (e.g. 10-70 W) (Hindley et al., 2004; Keserci & Duc, 2018; Liu et al., 2014; Stewart et al., 2003;

Zhu et al., 2016). When proceeding to the therapy sonications, the power can be adjusted according to the results of the previous sonications (Keserci & Duc, 2018). The therapy sonication is a volumetric sonication in which the ablated volume (i.e. therapy cell) is ellipsoidal (see Figure 4). During the therapy sonication, multiplane real-time thermometry maps are acquired and overlaid on magnitude images to monitor the heating of the target and adjacent tissues as presented in Figure 4 (Fennessy et al., 2007; Sridhar & Kohi, 2018; Zhu et al., 2016). From the thermometry images, the system can estimate automatically the lethal thermal dose-volume (240 CEM43 contours) which is demonstrated in Figure 4 (Kim et al., 2012).

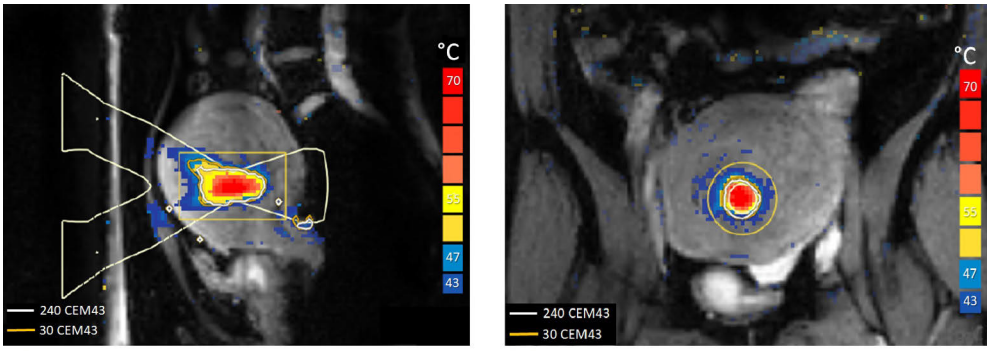

Figure 4. A case presentation of the real-time thermometry maps (presented as a color scale) overlaid on magnitude images (presented as grey scale) in a) sagittal and b) coronal direction at 3 tesla during the therapy sonication using 12 mm cell with power of 350 W resulting in maximum temperature of 73 ℃ and lethal thermal dose volume of 7.95 Ml. The imaging parameters were TE=19.5 ms, TR=37 ms, slice thickness= 7 mm, and field of view=400x400 mm.

To avoid thermal injury of adjacent tissues, such as skin burns, a cooling time between each therapy sonication is performed (Ellens & Hynynen, 2014; Rueff & Raman, 2013; Sridhar & Kohi, 2018). The cooling time depends on the size of the therapy cell i.e. the duration of the therapy sonication (Kim et al., 2015, 2012). The goal is to deliver therapy sonications in the target volume in a repetitive manner to achieve as large a non-perfused volume (NPV) as possible with respect to the uterine fibroid (Fennessy et al., 2007; Keserci & Duc, 2018).

Outcome assessment

Immediately after the MRgHIFU treatment, the outcome can be assessed with fat-saturated T1W CE images in which the ablated tissue can be seen as non-enhancing regions also known as non-perfused volume (NPV) (Fennessy et al., 2007; Kröncke

& David, 2019; Napoli et al., 2021; Sridhar & Kohi, 2018). The technical outcome is usually assessed with the non-perfused volume ratio (NPVr) which is defined as NPV divided by the total volume of the uterine fibroid that can be calculated from CE T1W and T2W images, respectively (Keserci & Duc, 2018;Kim et al., 2012; Rueff & Raman, 2013). Treatment outcome assessment from MR images is presented in Figure 5.

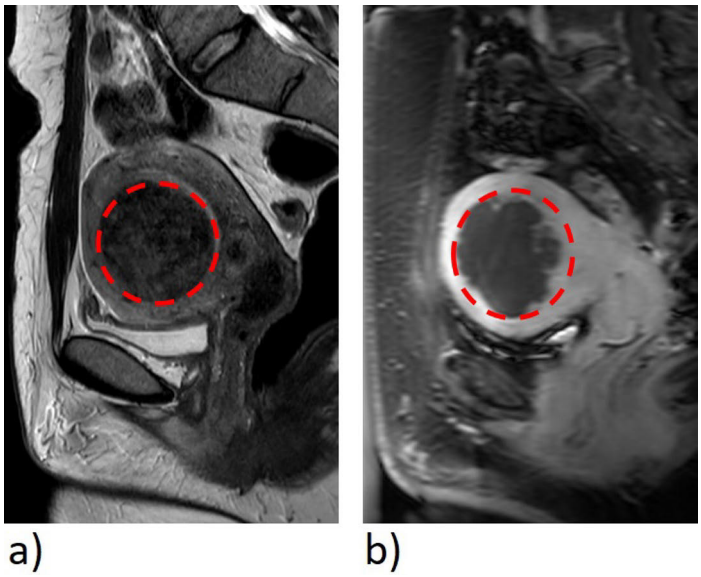

Figure 5. A case presentation of the assesment of the MRgHIFU treatment outcome from the 3 tesla MR images: a) the total volume of the uterine fibroid was 103 mL which was calculated from T2-weighted MR images (red dashed line), and b) non-perfused volume of the uterine fibroid was 85 mL which was calculated from T1-weighted contrast enhanced MR images, resulting in non-perfused volume ratio of 83% which is indicative of a good technical treatment outcome. The imaging parameters were a) TE= 95 ms, TR=4844 ms, slice thickness=3mm, and field of view=240x240 mm and b) TE=2.6 ms, TR=5.2 ms, slice thickness=3 mm, and field of view=250x345 mm.

Larger NPV ratios have been shown to correlate with the clinical outcome such as fibroid volume reduction and symptom improvements (Fennessy et al., 2007; Keserci & Duc, 2018; Mikami et al., 2008; Mindjuk et al., 2014;Park et al., 2014; Stewart et al., 2003, 2007; Tempany et al., 2003). An NPVr of more than 80% has been shown to result in clinical success in more than 80% of patients (Mindjuk et al., 2014). Correspondingly, the odds of clinical success have been shown to be 2.8 in those with an NPV of 30% or greater compared with those with an NPV of less than 30% (Fennessy et al., 2007).

Usually, the clinical outcome of the MRgHIFU treatment is assessed with symptom severity and/or quality of life questionnaires at different time points e.g.

before the treatment and at 3-months, 6-months, and 12 months after the treatment (Al Hilli & Stewart, 2010; Jolesz & Hynynen, 2007; Magalhães Peregrino et al., 2017). Spies et al. have described a specific questionnaire for uterine fibroids which is called the uterine fibroid symptoms quality of life (UFS-QOL) (Spies et al., 2002). The questionnaire addresses both the severity and frequency of the symptoms that are common in women suffering from uterine fibroids (Spies et al., 2002). The scale runs from 0-100 points and usually, women with symptomatic uterine fibroids have a mean score of 40 points (Jolesz & Hynynen, 2007; Spies et al., 2002). A common primary endpoint of successful clinical outcome is at least a 10 point reduction in the symptom severity score after the treatment (Al Hilli & Stewart, 2010; Stewart et al., 2006).

2.3 Magnetic resonance imaging (MRI)

Magnetic resonance imaging (MRI) is a widely used diagnostic imaging modality due to its superior soft-tissue contrast and the fact that it does not involve exposing the patient to ionizing radiation. MRI is based on the nuclear magnetic resonance (NMR) of the nuclei of the hydrogen atom (^{1}H) which consists of protons. Hydrogen atoms are present in water and fat molecules. Most soft tissues consist of up to 70-90% of water. MRI employs three different magnetic fields: the main static field of the scanner (B_0), spatial encoding gradients, and the oscillating magnetic field of the radiofrequency (RF) pulses (B_1). (Brown et al., 2014; McRobbie et al., 2017; Weishaupt et al., 2008)

The NMR is a quantum mechanical phenomenon; however, it can be described with classical mechanics. The main external magnetic field aligns the spins of protons with the field either in parallel or anti-parallel directions. The sum of all magnetic moments of the protons creates a net magnetization vector (M_0) parallel to the main magnetic field. In the B_0 –field, proton spins will undergo precession, like spinning tops, at a characteristic speed that is called the Larmor frequency (ω_0) which is directly proportional to the B_0 -field. To detect the MR signal, the net magnetization vector needs to be tilted into the transverse plane with an RF pulse which has the same frequency as the Larmor frequency (condition for NMR) which allows the proton spins to absorb the energy, a process also known as excitation. Immediately after the excitation, the net magnetization will start to return to the stable state (parallel to the B_0 -field) through two independent simultaneous processes: spin-lattice interaction and spin-spin interaction which are called T1 relaxation (longitudinal relaxation) and T2 relaxation (transverse relaxation), respectively. T1 relaxation time is the decay constant for the recovery of the longitudinal magnetization and T2 relaxation is the decay constant for the recovery of the transverse magnetization. (Brown et al., 2014; McRobbie et al., 2017; Weishaupt et al., 2008)

Different tissues have distinct T1 and T2 relaxation times, which allows contrast between tissues; this will be seen as relative brightness of different tissues in the MR images. The image contrast depends on the imaging parameters that enable the adjustment of so-called image weighting. The image can be T1-, T2- or proton density (PD) weighted. The contrast of T1W images is mainly determined by the T1 relaxation time of the tissues. In the T1W images, tissues with a short T_1 relaxation time are bright while tissues with a long T1 relaxation time are dark. The contrast of T2W images is primarily T2 relaxation time dependent so that tissues with a long T2 relaxation time are seen bright on T2W images while tissues with a short T2 relaxation time appear dark. The contrast of PD images is predominantly determined by the proton density of the tissues that are imaged. Typically, all MR images have contributions from all of these weightings; the primary weighting is determined by the imaging parameters. (Brown et al., 2014; McRobbie et al., 2017; Weishaupt et al., 2008)

The MR image formation is based on so called imaging sequences in which a number of radiofrequency pulses and gradients are applied in a particular setting for excitation, phase encoding, formation of the echo (i.e. MR signal), and collection of the MR signal. The most commonly used sequences are spin-echo (SE) and gradient echo (GRE). With these MRI sequences, desired image contrast can be scanned by changing the sequence parameters, such as echo time (TE), repetition time (TR), and flip angle. The TE refers to the time from the center of the RF pulse to the center of the echo. The TE defines the T2-weighting of the image so that as TE increases also the T2-weighting increases. The TR is the time between two RF pulses. The TR determines the T1-weighting of the image such that as the TR increases, the T1-weighting decreases. The PD-weighting can be achieved by minimizing the T1- and T2-weightnings and therefore, TE is short and TR is long in PD-weighted sequences. The SE sequence consists of a 90 degree RF pulse followed by a 180 degree RF pulse at half of the echo which produces an echo. The 180 degree refocusing pulse eliminates the effects of static magnetic field in homogeneities. In contrast, the GRE sequence consists of an RF pulse (typically below 90 degrees) and the echo is produced with dephasing and rephrasing gradients which are applied in the frequency encoding direction. (Brown et al., 2014; McRobbie et al., 2017; Weishaupt et al., 2008)

2.3.1 Quantitative MRI (QMRI)

The MRI scanner can be utilized not only for qualitative imaging but also to measure various tissue parameters such as the T1 relaxation time, T2 relaxation time, blood flow, and apparent diffusion coefficient (ADC) in a quantitative manner (McRobbie et al., 2017; Seiler et al., 2021;Tofts & Parker, 2013). Conventional MRI is a

qualitative imaging method because the signal intensity and image contrast are influenced by several imaging-related factors such as echo time, inversion time, repetition time, coil sensitivity, and gain effects (Bojorquez et al., 2017, 2019; Hardy et al., 1992). On the other hand, the quantitative MRI (QMRI) is largely independent on these factors and therefore, can provide more accurate and precise information about the physical properties of tissues (Bojorquez et al., 2019). Already in the earliest days of NMR and MRI, Raymond Damadian suggested that quantitative NMR parameters (T1 and T2 relaxation times) could be used for tissue characterization as normal tissue or cancerous tissue, as well as differentiating between benign and malignant tumours (Damadian, 1971). For example, the benefits of QMRI could be its more accurate and precise identification of biological changes in diseases and assessment of treatment responses (Serai, 2021).

In comparison with the MRI used in clinical routine, most QMRI techniques necessitate the acquisition of a series of weighted images with certain varying imaging parameters such as echo or inversion time which allow fitting of a mathematical model into the measured MR signal intensities voxel by voxel which can be transformed into quantitative parameter maps (Seiler et al., 2021). However, QMRI has not yet entered widespread clinical routine mostly due to the long acquisition times and its lack of reproducibility (Gulani & Seiberlich, 2020; Matzat et al., 2015). Nonetheless, a recent study demonstrated that the deviation of QMRI data acquired with the same and different scanners is low (Gracien et al., 2020). Novel acceleration techniques such as parallel imaging and sparse reconstruction methods could achieve shorter acquisition times for QMRI (Gulani & Seiberlich, 2020).

2.3.1.1 Dynamic contrast-enhanced (DCE) imaging

Dynamic contrast-enhanced magnetic resonance imaging (DCE-MRI) technique can provide quantitative information about tissue perfusion and permeability by using pharmacokinetic modelling in the analysis (Jackson et al., 2005; McRobbie et al., 2017;Tofts & Parker, 2013; Yankeelov & Gore, 2009). For example, DCE-MRI can be used in the quantitative characterization of tumours and in the evaluation of response to treatment (Khalifa et al., 2016;Tofts & Parker, 2013;Wei et al., 2017; Yankeelov & Gore, 2009). The DCE-MRI can also be used for predicting the MRgHIFU treatment outcomes of the uterine fibroids prior to the treatment because higher blood flow leads to greater heat dissipation from the targeted volume which can cause suboptimal treatment results (Kim et al., 2011, 2012, 2014; Li et al., 2020). The DCE-MRI consists of two main concepts to produce quantitative parametric maps: acquisition, and pharmacokinetic modelling (Jackson et al., 2005; McRobbie et al., 2017;Tofts & Parker, 2013; Yankeelov & Gore, 2009).

Acquisition

Determination of T1 relaxation time of the tissue prior to contrast agent (CA) injection is required to perform quantitative pharmacokinetic modeling of the DCE-MRI data in which the concentration of the CA is needed to be solved from the MR signal (Nam et al., 2017; Tietze et al., 2015;Tofts & Parker, 2013; Yankeelov & Gore, 2009). The T1 relaxation time of the tissue can be determined with a pre-bolus measurement of T1 relaxation time which is preferred but also a standard T1 relaxation time value from the literature can be used (Larsson et al., 2015; Nam et al., 2017; Tietze et al., 2015;Tofts & Parker, 2013). An error in T1 relaxation time measurement or if an incorrect literature value of T1 relaxation time is used, may well introduce gross errors in quantitative tissue parameters (Tofts & Parker, 2013).

The T1 relaxation time can be measured e.g. with variable flip angle (VFA) or inversion recovery (IR) techniques (Taylor et al., 2016; Tietze et al., 2015;Tofts & Parker, 2013). IR methods can give more accurate measurements of the T1 relaxation times compared to the VFA method, but usually IR methods are more time-consuming (Taylor et al., 2016; Tietze et al., 2015;Tofts & Parker, 2013). Thus, the VFA method is more commonly used in clinical setups due to its faster acquisition (Tietze et al., 2015;Tofts & Parker, 2013). The T1 relaxation time can be measured also with combined spin echo inversion recovery sequence consisting of a multiecho spin echo sequence interleaved wih a a multiecho inversion recovery sequence in which relaxation times can be calculated with ratios and least squares method (RLSQ) (in den Kleef & Cuppen, 1987). The measured ratios depend purely on T1 and T2 relaxation times (in den Kleef & Cuppen, 1987). The relaxation times are calculated from the measured ratios by an iterative technique (in den Kleef & Cuppen, 1987).

In the VFA method, gradient echo sequences are acquired with several different flip angles such as 5º, 10º, and 15º (Tietze et al., 2015;Tofts & Parker, 2013). The T1 relaxation time can be solved by fitting the data to Equation 3 when the TE is assumed to be much less than T2*:

$$\mathbf{S(\alpha)} = \boldsymbol{S_0} \cdot \frac{\boldsymbol{sin(\alpha)} \cdot [\mathbf{1} - \boldsymbol{e}^{(-\boldsymbol{TR/T1})}]}{\mathbf{1} - \boldsymbol{cos(\alpha)} \cdot \boldsymbol{e}^{(-\boldsymbol{TR/T1})}} \tag{3}$$

where $S(\alpha)$ is the measured signal intensity, α is the flip angle, S_0 is a constant describing the scanner gain and proton density, and TR is repetition time (Yankeelov & Gore, 2009). However, B_1 –field inhomogeneities may induce an offset to the calculated T1 relaxation time values and therefore, B_1 mapping is recommended for correcting for these possible offsets (Tietze et al., 2015;Tofts & Parker, 2013).

In the inversion recovery method, spin-echo sequences are acquired with different inversion times (TI) which refers to the time between the 180º inversion pulse and 90º excitation pulse (McRobbie et al., 2017;Tofts & Parker, 2013). From these images, the T1 relaxation time can be determined by using Equation (4) for the fitting:

$$\mathbf{S(TI)} = \boldsymbol{S_0} \cdot [\mathbf{1} - \mathbf{2} \cdot \boldsymbol{e}^{(-\boldsymbol{TI}/\boldsymbol{T1})} + \boldsymbol{e}^{(-\boldsymbol{TR}/\boldsymbol{T1})}] \quad (4)$$

where *S(TI)* is the measured signal intensity, *TI* is the inversion time, S_0 is a constant, and *TR* is repetition time (McRobbie et al., 2017). In both methods, the data can be fitted on a voxel-by-voxel basis which produces a T1 relaxation time map (Yankeelov & Gore, 2009).

The DCE-MRI data is acquired with a time series of a T1W gradient-echo sequence with high temporal resolution and optimal duration (Jackson et al., 2005;Tofts & Parker, 2013). The temporal resolution is usually around 2-5 seconds and the scanning duration is at least 5-10 minutes, both depending on the organ system of interest (Jackson et al., 2005;Tofts & Parker, 2013). During the acquisition, CA is injected into the bloodstream through a peripheral vein which is followed by a saline flush (Jackson et al., 2005; Khalifa et al., 2016;Tofts & Parker, 2013; Yankeelov & Gore, 2009). The bolus injection should be performed in a consistent manner with a power injector using flow rates around 2-4 mL/s, or the overall period of contrast administration should be kept constant such as 4 seconds followed by a saline flush of 20-30 mL with the same flow rate or at some time constant to create a coherent bolus into the systemic circulation (Jackson et al., 2005; Kim et al., 2011;Wei et al., 2017).

Pharmacokinetic modelling

To perform pharmacokinetic modelling, the CA concentration needs to be determined from the MR signal (Tofts & Parker, 2013). First, the reduction in T_1 from its native value (T_{10}) by the presence of a concentration of CA (c) can be found by the following relation:

$$\frac{\mathbf{1}}{\boldsymbol{T_1}} = \frac{\mathbf{1}}{\boldsymbol{T_{10}}} + \boldsymbol{r_1} \cdot \boldsymbol{c} \quad (5)$$

where r_1 is the longitudinal relaxivity of the CA (McRobbie et al., 2017;Tofts & Parker, 2013). Second, the signal increase by the T_1 reduction can be derived from Equation 3, when a spoiled gradient-echo sequence is used (Tofts & Parker, 2013). The concentration of CA in arterial blood plasma (C_p) is also required for pharmacokinetic modelling which can be derived from the concentration of CA in

arterial blood (C_a) which can be determined from the MR signal of blood (Tofts & Parker, 2013). The concentration of CA in plasma (C_p) is higher than the concentration of CA in whole blood (C_a) since the CA is only present in the plasma and blood contains also red blood cells which occupy a certain volume also known as the haematocrit (Hct), which can be measured (Tofts & Parker, 2013). Therefore, the relation between the concentration of CA in plasma and whole blood can be determined with Equation 6.

$$\boldsymbol{C_p(t) = \frac{C_a(t)}{1 - Hct}} \tag{6}$$

Nowadays, there are many different models that can be used to obtain a quantitative pharmacokinetic analysis e.g. Tofts model, extended Tofts model, Patlak model, and two-compartment exchange model which are based on modelling of the human body into one or more compartments in which the CA flows between these compartments (Patlak et al., 1983; S. Sourbron et al., 2009;Tofts & Kermode, 1989;Tofts, 1997). These models are based on different assumptions and therefore defined parameters change depending on which model is being used. The quantitative parameters that can be derived from the modelling are the transfer constant, which characterizes the diffusive transport of the CA across the capillary endothelium (K^{trans}), the volume of the extracellular space (v_e), and the rate constant, which describes the leakage of the CA from the extracellular space to the vascular compartment ($k_{ep} = K^{trans}/ v_e$), and when using more sophisticated models, also the blood flow (BF) and the vascular plasma volume (v_p) can be estimated (Tofts, 1997, 1999). However, depending on the model, the meaning of the rate constant differs because it can be affected by flow, permeability, endothelial surface area product, and proportional blood volume by the voxel (Jackson et al., 2005;Sourbron & Buckley, 2012, 2011). One of the most commonly used models is the extended Tofts model which is based on the bidirectional transfer of the CA between two-compartments as illustrated in Figure 6 (Chen et al., 2011).

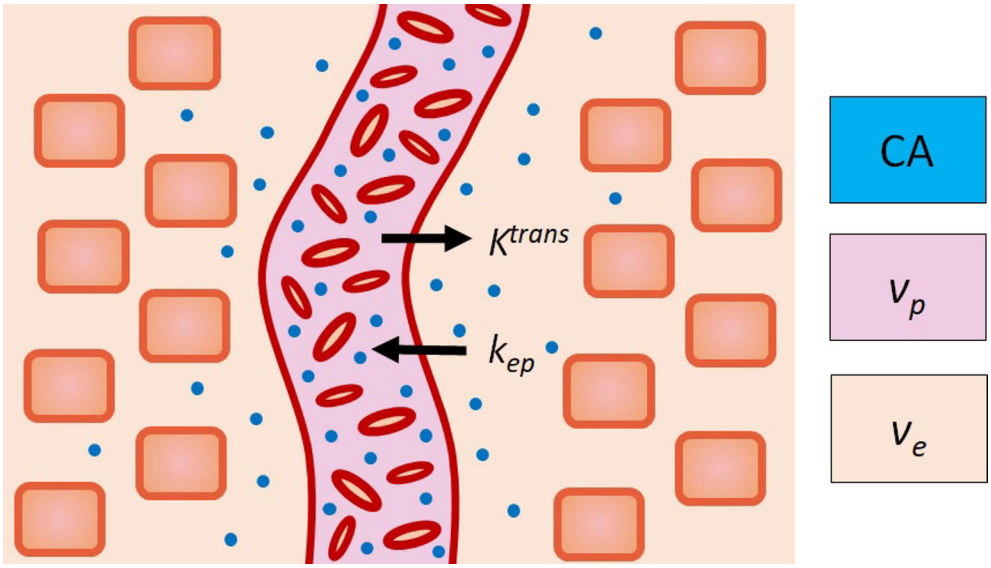

Figure 6. An illustration of the bidirectional transfer of the contrast agent (CA) in the extended Tofts model between the arterial plasma volume (v_p) and the extracellular volume (v_e) with the transfer constant (K^{trans}) and the rate constant (k_{ep}).

In the extended Tofts model, the parameters K^{trans}, k_{ep}, v_e, and v_p are estimated by the following formula:

$$\boldsymbol{C_t(t) = C_p(t) \cdot v_p + K^{trans} \cdot \int_0^t C_p(\tau) \cdot e^{-(K^{trans}/v_e)\cdot(t-\tau)}\, d\tau} \qquad (7)$$

where C_t and C_p are the CA concentrations in the tissue and plasma, K^{trans} is the transfer constant, v_e, and v_p are the fractional volumes of extracellular space and plasma (Tofts, 1997).

It is possible to estimate tissue blood flow (*BF*) in two ways 1) the two-compartment exchange model (2CM) or 2) bolus passage perfusion estimate (Sourbron & Buckley, 2011;Tofts & Parker, 2013; van Osch, 2013). The bolus passage perfusion analysis is restricted to early phase CA delivery to the tissue when usually the effects of CA leakage can be ignored or assumed to be unidirectional (Tofts & Parker, 2013). In the first passage of the bolus, the parametric blood flow (*BF)* values can be obtained by deconvolution arithmetic with the first pass of the measured CA concentration in the voxel (*Cvoxel)* and the arterial input function (AIF) curve (Equation 7) (van Osch, 2013). The blood flow can be obtained from Equation 8, as a scaling factor of the residue function (*R(t)*) by using a literature value for the ratio of large and small vessel haematocrit, after noting that *R(0)=1* (i.e. all of the CA remains in the voxel at time zero) (van Osch, 2013).

$$\boldsymbol{C_{voxel}(t) \otimes^{-1} AIF(t) = BF \cdot \frac{1 - Hct_{small\ vessel}}{1 - Hct_{large\ vessel}} \cdot R(t)} \quad (8)$$

Determination of the arterial input function (AIF), which is also known as the arterial plasma concentration (C_p), is needed for the pharmacokinetic modelling on a voxel by voxel basis or through individual regions of interest (ROIs) (Tofts & Parker, 2013). The AIF describes the changes in the CA concentration in the intravascular plasma as a function of time (Khalifa et al., 2016). The AIF can be measured from the afferent artery to the tissue of interest in the DCE-MRI data but also population-based AIF can be used (Cuenod & Balvay, 2013; Khalifa et al., 2016; Tofts & Parker, 2013). From a small population of subjects, the AIF can be measured individually by taking a series of arterial blood samples from which the CA concentration can be determined and an average AIF of the subjects can be used in future studies as a population-based AIF. Individually measured AIF takes into account variations between and within-subjects. However, if it is not implemented properly it can introduce variation into the analysis which can result in the production of implausible v_e values (>100%) (Cuenod & Balvay, 2013; Hadizadeh et al., 2017; Khalifa et al., 2016; Tofts & Parker, 2013).

2.3.1.2 Diffusion-weighted imaging (DWI)

Diffusion-weighted imaging (DWI) is a widely exploited quantitative MR imaging technique with several clinical applications also in visualizing brain and abdominal pathology (Boto et al., 2018; Mannelli et al., 2015). DWI is based on measuring the random Brownian motion of water molecules within a voxel of tissue and therefore, the technique can provide information on the structures and processes at the tissue level, such as cellularity and microcirculation (Feuerlein et al., 2009; Kele, 2010; Morani, 2013). Therefore, DWI can be used in characterization of uterine fibroids (Andrews et al., 2019; Shimada et al., 2004; Verpalen et al., 2020). DWI can be exploited also to monitor ablated uterine fibroid tissue during the MRgHIFU treatment because ablation evokes changes at the tissue level (Ikink et al., 2014; Jacobs et al., 2010; Pilatou et al., 2009).

The DWI sequence consists of a conventional spin-echo sequence with two strong gradients also known as diffusion gradients located between 90º and 180º RF pulses and after 180º RF pulse before the signal readout at the echo time (TE) as presented in Figure 7 (Sigmund & Jensen, 2011; Stejskal & Tanner, 1965).

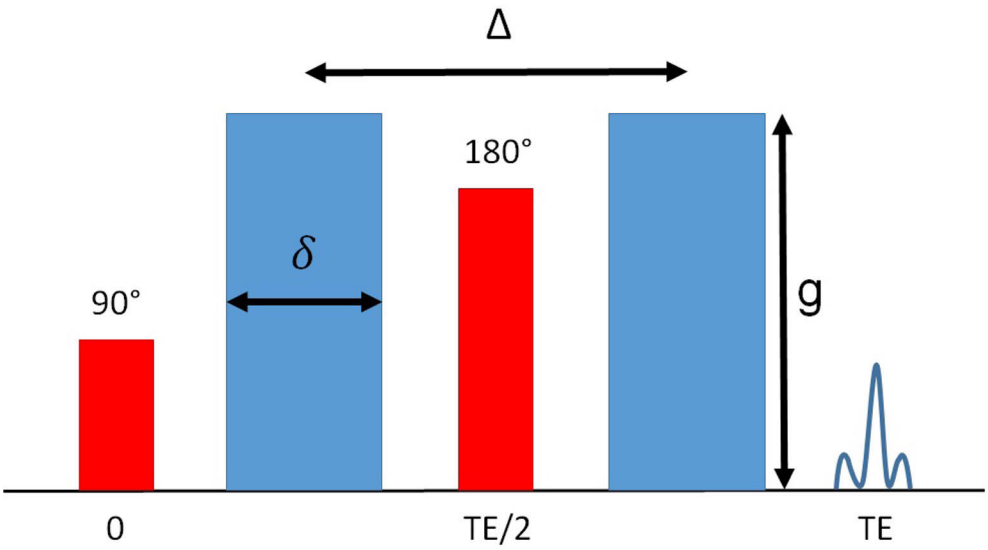

Figure 7. An illustration of the DWI sequence, where red columns represent the RF pulses and blue columns represent the diffusion gradients at different time points in respect of the echo time (TE). Parameters related to the diffusion gradients are also presented: δ is the pulse duration, g is the magnitude of the diffusion gradient, and Δ is the diffusion time.

With these diffusion gradients, the signal can be sensitized to molecular diffusion so that they do not affect the signal magnitude if the spins are stationary but if the spins move due to molecular diffusion a measurable signal loss can be detected in the direction of diffusion gradients (Sigmund & Jensen, 2011). Different diffusion weightings also known as b-values can be defined by the strength and timing of the diffusion gradients according to Equation 9 (Sigmund & Jensen, 2011; Stejskal & Tanner, 1965).

$$\mathbf{b} = (\boldsymbol{\gamma} \cdot \boldsymbol{\delta} \cdot \boldsymbol{g})^{\mathbf{2}} \cdot (\Delta - \frac{\boldsymbol{\delta}}{\mathbf{3}}) \tag{9}$$

In Equation 9, b is the so-called b-value, γ is the gyromagnetic ratio, δ is the pulse duration, g is the magnitude of the diffusion gradient, and Δ is the diffusion time which are also illustrated in Figure 7 (Sigmund & Jensen, 2011). In clinical practice, usually b-values range between 0 and 1000 s/mm^2 but also larger b-values can be utilized; in the detection of prostate cancer, the largest b-value used is 2000 s/mm^2 (Jambor et al., 2019; Sigmund & Jensen, 2011).

The resulting signal attenuation of diffusion weighting can be calculated by the following equation which applies with Gaussian diffusion:

$$\mathbf{S(b)} = \boldsymbol{S_0} \cdot \boldsymbol{e^{-b \cdot D}} \quad (10)$$

where S is the signal intensity, S_0 is the signal intensity without diffusion weighting (diffusion gradients), b is the b-value, and D is the diffusion coefficient in the direction of the diffusion gradients (Sigmund & Jensen, 2011; Srivastava et al., 2008). However, in biological tissues diffusion may be significantly non-Gaussian and the previous equation is not valid (Sigmund & Jensen, 2011; Srivastava et al., 2008). The diffusion coefficient also depends to some extent on imaging parameters such as the echo time and diffusion time. The diffusion measurements of biological tissues are also affected by blood flow which can be misinterpreted as diffusion (Sigmund & Jensen, 2011). For these reasons, the true diffusion coefficient cannot be calculated in clinical DWI (using Equation 10), and the diffusion coefficient is usually denoted as apparent diffusion coefficient (ADC) in clinical routine (Sigmund & Jensen, 2011; Srivastava et al., 2008).

In the DWI sequence, a series of images are acquired with different b-values, and from these b-value images, ADC maps can be reconstructed on a voxel-by-voxel basis by using Equation 9 (Sigmund & Jensen, 2011). The ADC value can depend on several factors e.g. cellularity, extracellular fluid quantity, and perfusion because ADC values in biological tissues reflect diffusion in all its different compartments: extracellular, intracellular, and intravascular space (Sbano & Padhani, 2011). The decrease in the diffusion signal originating from the intravascular space attenuates more rapidly, due to perfusion, than that from the intra- and extracellular spaces. Therefore, in some cases, the ADC values can provide information about perfusion when ADC maps are reconstructed from low b-value (0–200 s/mm^2) DW images (Babsky et al., 2011; Ikink et al., 2014; Le Bihan et al., 1988; Sigmund & Jensen, 2011; Thoeny et al., 2004). The choice of b-value images used for ADC map calculation has been shown to influence the ADC values measured from the uterine fibroid tissue, which suggests that the DWI of the uterine fibroids may reflect both diffusion and perfusion effects (Ikink et al., 2014).

2.3.1.3 T2 relaxation time mapping

T2 relaxation time mapping is a quantitative MRI technique in which the T2 relaxation time of the tissue is measured (Serai, 2021). T2 relaxation time mapping can provide quantitative information about characteristics such as fiber content, iron content, and water content in different tissues (Barrera et al., 2019; Hänninen et al., 2017; Mosher & Dardzinski, 2004; Nissi et al., 2006; Swe et al., 1992; Verpalen et al., 2020; Welsch et al., 2014). In the clinical routine, T2 relaxation time mapping can be used for an assessment of the liver's iron content (Serai, 2021). T2 relaxation

time maps can be calculated using a spin echo sequence with different echo times by the following equation:

$$\mathbf{S(TE)} = \boldsymbol{S_0} \cdot \boldsymbol{e^{-(TE/T2)}} \quad (11)$$

where S is the signal intensity, S_0 is the signal intensity at TE=0, TE is the echo time, and T2 is the transversal relaxation time (Papanikolaou et al., 2002; Serai, 2021; Sharafi et al., 2018; Verpalen et al., 2020). In addition to the monoexponential T2 relaxation time method, also biexponential and multiexponential T2 time methods have been used for separating different compartments of tissues, e.g. in the brain, three water components can be detected: myelin water, intra- and extracellular water, and cerebrospinal fluid (Nikiforaki et al., 2020; Papanikolaou et al., 2002; Reiter et al., 2009; Sharafi et al., 2017, 2018; Whittall et al., 1997).

The acquisition of a spin echo sequence using only one refocusing pulse is too time-consuming for clinical use and sensitive to the diffusion effects (Nöth et al., 2017). Faster methods, such as the Carr-Purcell-Meiboom-Gill (CPMG) sequence, employ a series of refocusing pulses applied with a constant spacing (i.e. echo spacing) so that spin echoes are sampled with increasing echo times which are multiples of the echo spacing as illustrated in Figure 8 (Carr & Purcell, 1954; McRobbie et al., 2017; Nöth et al., 2017). The CPMG sequence compensates for diffusion effects and the accumulation of imperfections in the 180º pulses over the echo train (McRobbie et al., 2017). However, imperfections in the 180º pulse can lead to variations in the pulse heights so that the first and every odd-numbered pulse will be slightly too small, but the even-numbered echoes will be the correct height (McRobbie et al., 2017). However, the acquisition time of a CPMG sequence is approximately 15 minutes which is too long for routine clinical use (Quaia et al., 2008). The acquisition time can be further decreased by using for example a gradient echo and spin echo (GRASE) sequence, which combines turbo spin echo (TSE) and echo-planar imaging (EPI) methods by using a train of refocusing 180° pulses and additional gradient echoes for each spin echo of the readout gradient (Oshio & Feinberg, 1991; Quaia et al., 2008). T2 relaxation times measured with GRASE sequence have demonstrated good correlation with CPMG and TSE sequences (Fernández-Jiménez et al., 2015; Sprinkart et al., 2015). However, T2 relaxation time values have been shown to depend on sequence type of which CPMG is usually considered as a reference sequence (Mars et al., 2018; Quaia et al., 2008).

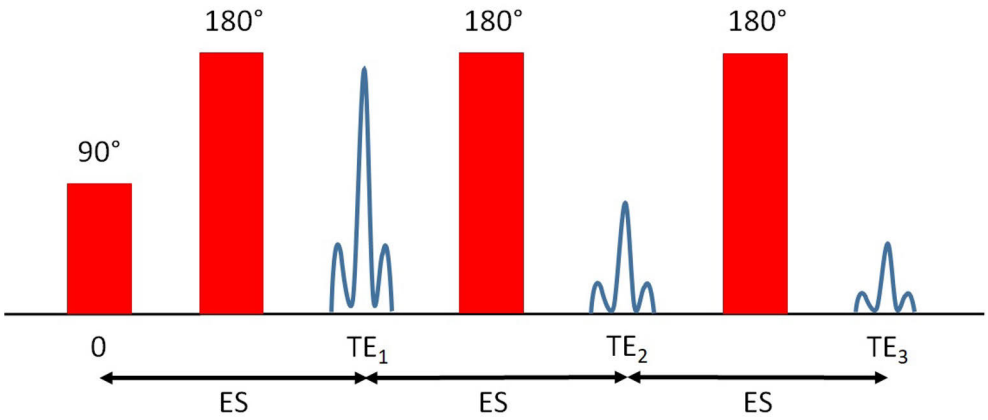

Figure 8. An illustration of the CPMG sequence, where red columns represent the RF pulses with respect to increasing the echo times (TE) with constant echo spacing (ES).

3 Aims

The aims of this doctoral thesis were to investigate the feasibility of applying quantitative magnetic resonance imaging (QMRI) techniques in magnetic resonance-guided high-intensity focused ultrasound (MRgHIFU) treatment of uterine fibroids, with a special emphasis on the technical prediction of the treatment outcome as well as examining the effects of oxytocin on the blood flow. The specific aims were:

I. to exploit dynamic contrast-enhanced magnetic resonance imaging to study the effects of oxytocin infusion on the blood flow of different types of uterine fibroids and the surrounding tissues as compared to baseline.

II. to investigate the feasibility of apparent diffusion coefficient in predicting the technical outcome of MRgHIFU treatment of uterine fibroids, and to compare it with the existing evaluation method: Funaki classification.

III. to examine the feasibility of T2 relaxation time in predicting the technical outcome of MRgHIFU treatment of uterine fibroids, and to compare it with existing evaluation methods: Funaki and SSI classifications.

4 Materials and Methods

4.1 Phantoms

In study III, the T2 relaxation time mapping sequence and fitting software of the scanner (Philips) were validated using a set of aqueous paramagnetic relaxation phantoms. Four solutions were prepared as described in a previous study (Thangavel & Saritaş, 2017). Solutions were prepared in centrifuge tubes of 50 millilitres by dissolving copper sulfate pentahydrate ($CuSO4 \cdot 5\ H2O$, purity ≥ 98%, Sigma-Aldrich) in double distilled water with concentrations of 26.905 mM, 19.359 mM, 13.341 mM and 4.482 mM resulting in T2 relaxation times of 50 ms, 69 ms, 99 ms, and 275 ms, which represent T2 relaxation times of skeletal muscle, white matter, grey matter and blood at 3 Tesla, respectively. The concentrations and T2 relaxation times were defined from a previous study (Thangavel & Saritaş, 2017). Furthermore, the influence of different coil set-ups on the measured T2 relaxation times was assessed with the phantoms.

4.2 Patients

In study, I, a total of 17 premenopausal women with one or several fibroids and 11 women without uterine fibroids, referred to here as healthy volunteers were enrolled in this study. The inclusion criteria were symptoms caused by uterine fibroids, mental and physical health appropriate for an MRI scan, and premenopausal status. Exclusion criteria were an ischemic heart condition, high blood pressure, a known allergy to Syntocinon medicine or any of its adjuvants, a long QT- syndrome, or any medication that prolongs the QT interval.

In study II, a total of 42 patients were included from the 64 patients who underwent the MRgHIFU treatment of uterine fibroid(s) between May 2016 and December 2018 in the Turku University Hospital. The exclusion criteria were: 1) oxytocin infusion was used during the MRgHIFU treatment (N=14), 2) patient had not undergone DWI prior to the MRgHIFU treatment (N=4), 3) there were significant artifacts on the ADC map which prevented to reliably measure the mean ADC value from the uterine fibroid (N=1), 4) treatment efficiency parameters could

not be identified for each treated fibroid (N=2), and 5) the MRgHIFU treatment hadbeen interrupted (N=1).

In study III, a total of 30 patients were examined from the 46 patients who had undergone the MRgHIFU treatment of uterine fibroid(s) between April 2017 and December 2018 in the Turku University Hospital. The exclusion criteria were: 1) patient had not undergone T2 relaxation time mapping prior to the MRgHIFU treatment (N=0), 2) oxytocin infusion was used during the MRgHIFU treatment (n=13), and 3) the MRgHIFU treatment could not be conducted without interruptions or obstacles (N=3).

Study I was performed in accordance with the ethical regulations of the Ethics Committee of the Hospital District of Southwest Finland and the National Committee of Medical Research Ethics (T366/2017 25.1.2018). Written informed consent for the MRI and oxytocin administration was obtained from all patients and healthy volunteers in study I. For studies II and III, approval by the Ethics Committee of the Hospital District of Southwest Finland (ETMK: 95/1801/2015 16.6.2015) was obtained. Written informed consent for the MRgHIFU procedure was obtained from all patients in studies II and III.

4.3 Equipment

In the study, I, all participants were examined with the same MRI scanner (Ingenia 3.0 T, Philips, Best, The Netherlands) using a 32-channel dStream torso coil.

In studies II and III, the screening MRI was performed with different scanners because patients were referred to the Turku University Hospital also from other hospitals in Finland. Twenty-five patients in study II and 15 patients in study III had their screening MRI performed with the same MRI scanner (Ingenia 3.0 T, Philips Healthcare, Best, The Netherlands) using a 32-channel dStream torso coil in the Turku University Hospital.

In studies II and III, all the MRgHIFU treatment procedures were performed using the same extracorporeal, clinical tabletop MRgHIFU system (Sonalleve V2, Profound Medical Inc., Mississauga, Canada) equipped with a direct skin cooling device in combination with a 3.0T clinical MR scanner (Ingenia, Philips, Best, the Netherlands).

4.4 Imaging protocols

In study I, an extensive MRI protocol was acquired for each woman in a prone position. The MRI scan protocol was performed with and without continuous oxytocin infusion at Turku University Hospital on different days. The imaging protocol included T2W, T1W, spin echo inversion recovery for T1 relaxation time analysis, and contrast-

enhanced T1W imaging, and dynamic contrast-enhanced (DCE) imaging for quantitative perfusion analysis. The spin echo inversion recovery sequence parameters were TE=11 ms, TR/SE=1133 ms, TR/IR=1733 slice thickness=3 mm, inversion delay=600 ms, and field of view=270x349 mm. The DCE sequence included 70 time frames (i.e. dynamics) acquired with a temporal resolution of 4.3 seconds. The imaging parameters of DCE sequence were TE=1.3 ms, TR=2.9 ms, slice thickness=6 mm, flip angle=10°, and field of view=270x349 mm. A single dose of contrast agent (Dotarem, Guebert, Roissy, France) was injected at a constant rate after the acquisition of the first five dynamic scans followed by a saline flush.

In study II, the screening MRI protocol in our hospital included T2W, T1W, diffusion-weighted, and contrast-enhanced T1W imaging. The screening MRI protocol applied in other hospitals usually included T2W, T1W, and contrast-enhanced T1W imaging with slightly varying sequence parameters. The diffusion-weighted imaging was performed during screening MRI using a torso coil setup with 32 channels or before the MRgHIFU treatment with a HIFU coil system; this consists of two coils with a total of 5 channels. The DW images were acquired with b-values of 0, 100, 400, 600, and 800 s/mm^2. The imaging parameters of DWI sequence were TE=83 ms, TR=3733 ms, slice thickness=5 mm, and field of view=290x375 mm.

In study III, the screening MRI protocol in our hospital included T2W, T1W, T2 relaxation time mapping, and contrast-enhanced T1W imaging. The screening MRI protocol utilized in other hospitals usually included T2W, T1W, and contrast-enhanced T1W imaging with slightly varying sequence parameters. The T2 relaxation time mapping was performed during screening MRI using a torso coil setup with 32 channels or before the MRgHIFU treatment with a HIFU coil system that consists of two coils with a total of 5 channels. T2 relaxation time mapping was acquired with a multi-echo, turbo spin-echo (TSE), echo-planar imaging (EPI) based technique by acquiring images with 16 echo times with constant echo spacing (12-192 ms). The imaging parameters of T2 relaxation time mapping sequence were TR=2800 ms, slice thickness=5 mm, and field of view=183x230 mm.

Detailed description of imaging parameters can be found in the original publications.

4.5 Image analysis

In all studies, the Funaki classification was determined for all fibroids by drawing ROIs on the screening MRI T2W image. A round ROI was placed so as to cover most of the fibroid and elliptical ROIs were positioned on the myometrium and the abdominal muscle while avoiding partial volume effects. Average signal intensity values for all three ROIs were obtained and compared in order to determine the Funaki type of each fibroid.

In study II, relative T2W signal intensities (rT2) were determined for the correlation analysis as continuous parameters of the Funaki classification. The average signal intensity of the fibroid divided by the average signal intensity of skeletal muscle was denoted as rT2(fibroid/muscle) and the average signal intensity of fibroid divided by the average signal intensity of myometrium was denoted as rT2(fibroid/myometrium).

In study III, the scaled signal intensity (SSI) was determined for all fibroids by drawing ROIs on the screening MRI T2W image. A round ROI was placed to cover most of the fibroid and elliptical ROIs were positioned on the abdominal subcutaneous fat and the abdominal muscle while avoiding partial volume effects. Average signal intensity values for all three ROIs were obtained and scaled between 0 and 100 in order to determine the SSI of each fibroid.

In study I, The T1 relaxation time maps were reconstructed using the MRI scanner software (Philips). The ROIs were drawn in three middle slices of the fibroid and an averaged quantitative T1 relaxation time values were obtained for each fibroid.

In study I, the DCE-MRI data was analyzed with NordicICE software version 4.1.1 (NordicNeuroLab AS, Bergen, Norway). The arterial input function was determined from the internal iliac artery by placing a circular ROI onto the artery lumen. Parametric blood flow values were obtained by T1 perfusion deconvolution arithmetic with the first pass of the AIF curve. Averaged blood flow values were obtained from the ROIs of the fibroids, the myometrium, and the abdominal muscle.

In study II, the ADC maps were reconstructed from the diffusion-weighted images acquired in three orthogonal directions for quantitative analysis using the MRI scanner software (Philips). The ACD maps were calculated with different combinations of b-values: 1) all b-values, 2) the lowest two b-values to emphasize the perfusion effects (0 and 100 s/mm2), and 3) the highest b-values to capture the diffusion effects (400, 600, and 800 s/mm2). ROIs were drawn in the three middle slices of the fibroid to include most of the fibroid while avoiding the partial volume effect. The ROIs were then copied to all ADC maps in the same three sequential slices, and averaged quantitative ADC values were obtained from each ADC map.

In study III, The T2 relaxation time maps were reconstructed using the MRI scanner software (Philips). The ROIs were drawn in three middle slices of the fibroid and an averaged quantitative T2 relaxation time values were obtained for each fibroid.

In studies II and III, the technical treatment outcome i.e. NPVr was determined by computing volumes for the NPV and the uterine fibroid from the T1W contrast-enhanced and the T2W images, respectively, using a manual segmentation tool available in the image analysis software (AW- server 3.2, GE Healthcare).

4.6 MRgHIFU treatment efficiency analysis

In study II, the heating and ablation efficiencies of the MRgHIFU treatment of the uterine fibroids were investigated for each fibroid. The heating efficiency was defined as the total volume of 240 CEM43 contours divided by the total volume of treatment cells (%), and the ablation efficiency was defined as the non-perfused volume divided by the total volume of treatment cells (%).

A novel way to define heating efficiency was devised in this study; in this approach, the total volume of 240 CEM43 contours was divided by the total delivered acoustic energy at the focus (mL/J) per treatment. The described heating efficiency was not dependent on the cell type, the therapy power used, or the patient's anatomy. In order to determine the total delivered acoustic energy at the focus, an attenuation correction was estimated by determining the ultrasound attenuation for each layer.

4.7 Statistical analysis

In all studies, statistical analysis was performed using JMP Pro statistical software version 13.1.0 (SAS Institute Inc.). All datasets were analyzed for normal distribution with the Shapiro–Wilk W test and a p-value less than 0.05 was considered statistically significant in all studies.

In study I, the blood flow values of different tissues with and without oxytocin infusion were compared with the Tukey–Kramer test for all pairs or with a nonparametric Steel–Dwass method for all pairs depending on the distribution of the datasets. In addition, a retrospective power analysis was performed using standard least squares to ensure that there had been a sufficient number of patients in the fibroid group.

In study II, correlations between the pretreatment values of the uterine fibroids and the treatment parameters were assessed with nonparametric correlation analysis. Optimal ADC cut-off values were determined for the classification with receiver-operating-characteristic (ROC) curve analysis. The ADC classification was compared to the Funaki classification using ROC curve analysis and statistical significance was tested with the Chi-square test.

In study III, a correlation between the pretreatment values of the uterine fibroids and the treatment outcomes was assessed with nonparametric statistical measures. Optimal T2 relaxation time cut-off values were determined for classifications with ROC curve analysis. The T2 relaxation time classifications were compared to the Funaki classification and the SSI classification using ROC curve analysis and statistical significance was tested with the Chi-square test.

5 Results

5.1 Effect of oxytocin on the blood flow of the uterine fibroids, myometrium, and skeletal muscle (Study I)

Oxytocin infusion decreased significantly the blood flow of all the uterine fibroids analyzed. The measured blood flow values of the uterine fibroids without and with oxytocin infusion are presented in Figure 9.

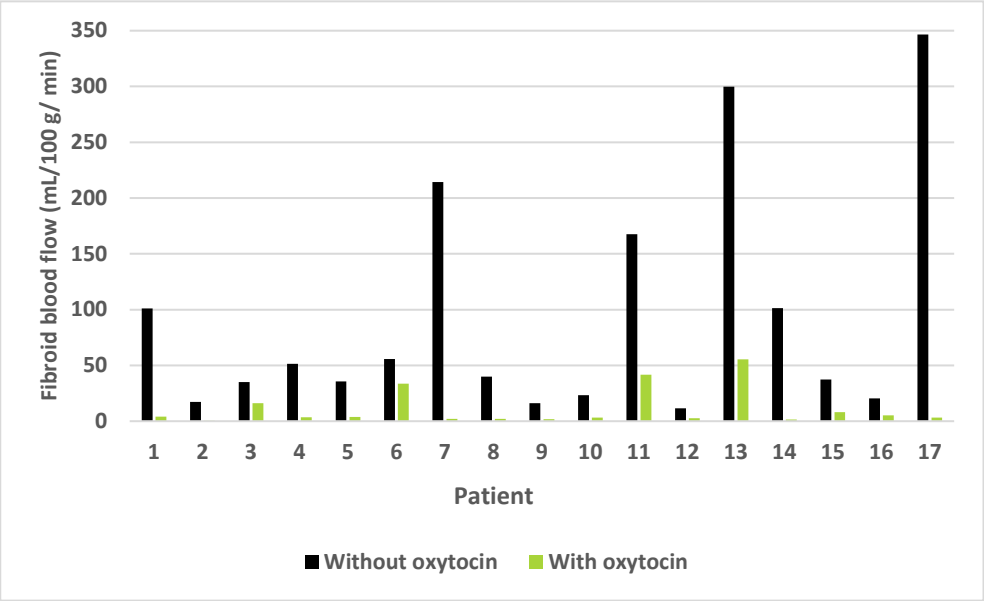

Figure 9. Bar chart of the measured blood flow values of the uterine fibroids without and with oxytocin infusion for each patient. Modified from study I.

Oxytocin statistically significantly decreased the blood flow of the uterine fibroids. Oxytocin exerted no statistically significant effect on the blood flow of the myometrium in either the fibroid group or the control group. Oxytocin had a minor,

although statistically significant effect on the skeletal muscle blood flow by increasing it. The summary of median blood flow values in both groups without and with oxytocin infusion is presented in Table 1.

Table 1. Summary of blood flow values for the fibroid group and the control group without and with oxytocin infusion presented as median [interquartile range].

	Fibroid group		Control group	
	Without oxytocin	With oxytocin	Without oxytocin	With oxytocin
Fibroid blood flow (mL/100g/min)	39.9 [21.9–134.5]	3.5 [2.1–12.1] *	NA	NA
Myometrium blood flow (mL/100g/min)	61.1 [26.4–165.2]	69.4 [21.5–101.4]	59.4 [43.6–109.2]	68.6 [30.8–101.4]
Muscle blood flow (mL/100g/min)	2.1 [1.6–2.8]	3.7 [2.7–5.3] *	2.0 [1.6–4.4]	4.9 [3.2–6.3] *

* p-value < 0.05, tested with nonparametric measures between blood flow values without and with oxytocin.

All the women in the study tolerated the oxytocin infusion without any reported symptoms and no side effects were observed. The oxytocin infusion had no marked effect on the blood pressure or heart rate of the women.

5.2 The feasibility of ADC in predicting the technical outcome of MRgHIFU treatment of uterine fibroids (Study II)

The ADC maps were reconstructed with different combinations of b-values resulting in median ADC value of 1103 x 10^{-6} mm^2/s and interquartile range of 943–1188 x 10^{-6} mm^2/s with all b-values, 977 x 10^{-6} mm^2/s and interquartile range of 848-1055 x 10^{-6} mm^2/s with the highest b-values, and the mean ADC value of 2576 ± 812 x 10^{-6} mm^2/s with the lowest b-values.

Correlation analysis between the five pretreatment MRI parameters and treatment parameters showed that only ADC with the lowest b-values displayed a significant correlation with heating efficiency (%) and only rT2(fibroid/muscle) exhibited a significant correlation with the heating efficiency (mL/J). None of the pretreatment parameters correlated with the ablation efficiency. Four pretreatment parameters correlated significantly with the NPVr: ADC with all and the highest b-values, rT2(fibroid/muscle) and rT2(fibroid/myometrium).

Based on the correlation analysis the ADC with all b-values was chosen for the classification analysis. The optimal cutoff values of the ADC with all b-values were determined with ROC curve analysis resulting in cutoff values of $980x10^{-6}$ mm^2/s and $1800x10^{-6}$ mm^2/s which correspond to treatment results of NPVr > 80% and NPVr < 30%, respectively. The resulted ADC classification was ADC I (NPVr > 80%), ADC II (NPVr 30–80%), and ADC III (NPVr < 30%).

A comparison of group means of NPVr with all pairs with Tukey–Kramer honestly significant difference test revealed a statistically significant difference between ADC classification groups whereas there were no significant differences between Funaki classification groups (Figure 10).

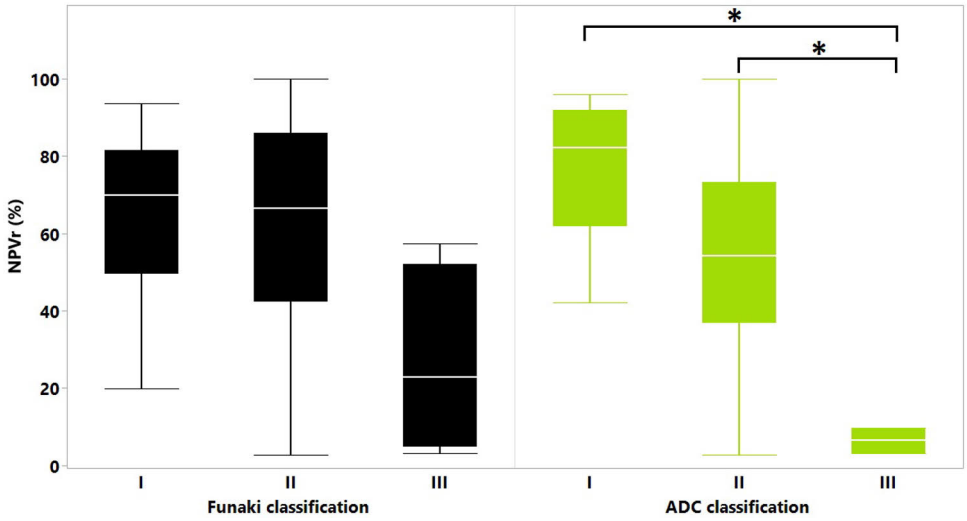

Figure 10. Box-Wisker plots presenting NPVr (%) for the Funaki classification and the ADC classification groups where asterisk presents p-value < 0.05. Modified from study II.

The classifications were compared using ROC curve analysis (Figure 11). The ADC classification resulted in the whole model area under the curve (AUC) value of 0.79 (p-value = 0.0007), whereas the AUC for the Funaki classification was 0.62 (p-value = 0.0527) in predicting the NPVr.

Linear regression analysis of the total volume of 240 CEM43 contours and the total delivered acoustic energy at the focus for each classification group showed a statistically significant regression effect for ADC I, ADC II, Funaki I, and Funaki II classification groups.

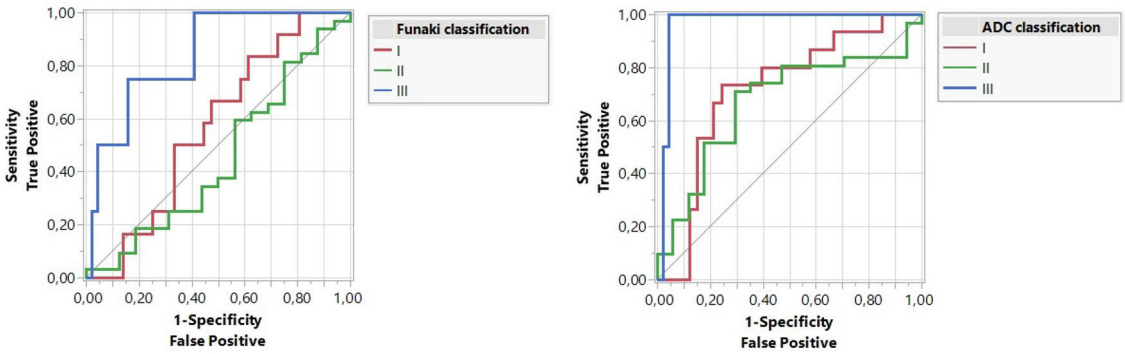

Figure 11. ROC curves by the NPVr (%) for the Funaki classification and the ADC classification groups where the area under curve values for each classification group were ADC I 0.72, ADC II 0.67, ADC III 0.97, Funaki I 0.57, Funaki II 0.45, and Funaki III 0.84. Modified from study II.

5.3 The feasibility of T2 relaxation time in predicting the technical outcome of MRgHIFU treatment of uterine fibroids (Study III)

The T2 relaxation time phantoms were measured with the HIFU coil and the torso coil setup to validate the T2 relaxation time mapping sequence and fitting software. Validation measurement results for each relaxation time phantom are presented in Table 2.

Table 2. T2 relaxation time validation measurement results for each relaxation time phantom with both coil setups. Modified from study III.

	HIFU coil		Torso coil	
Phantom	**Measured T2**	**Difference**	**Measured T2**	**Difference**
50 ms	51.039 ms	+2.1 %	50.038 ms	+0.1 %
69 ms	69.552 ms	+0.8 %	68.051 ms	-1.4 %
99 ms	100.575 ms	+1.6 %	98.073 ms	-0.9 %
275 ms	293.717 ms	+6.8 %	285.210 ms	+3.7 %

A correlation analysis between the pretreatment MRI parameters and treatment parameters showed that T2 relaxation time, rT2(fibroid/muscle), rT2(fibroid/myometrium) and SSI had all statistically significant negative correlation with NPVr resulting in the following correlation coefficients and p-values: -0.54 (p-value 0.001*), -0.37 (p-value 0.035*), -0.47 (p-value 0.007*), and -0.37 (0.035*), respectively.

Two different classification analyses were performed for the T2 relaxation time values, resulting in classification groups of T2 I (NPVr >80%), T2 II (NPVr 30–80%), and T2 III (NPVr <30%) when comparing to the Funaki classification and T2 I (NPVr>45%), and T2 II (NPVr≤45%) when compared to the SSI classification. The optimal cut-off values T2 relaxation time values were determined with the ROC curve analysis resulting in cutoff values of 57.6 ms for NPVr>80%, 78.3 ms for NPVr <30%, and 68.0 ms for NPVr >45%.

The T2 classifications were compared to the Funaki classification and the SSI classification with the Steel-Dwass method for all pairs and with the Tukey-Kramer honestly significant difference test for all pairs, respectively. There was no statistical difference between the Funaki classification groups or the SSI classification groups; whereas there were statistically significant differences between the T2 classification groups (Figure 12).

The classifications were compared using ROC curve analysis, which showed that the T2 classifications had higher sensitivity, specificity, and AUC values for each group compared to the Funaki classification and SSI classification groups in predicting the NPVr. The Chi-square test of the T2 classifications resulted in the whole model p-value of p-value = 0.0019* and p-value = 0.0024*, whereas the p-value for the Funaki classification was 0.56 and for the SSI classification was 0.0749 in predicting the NPVr.

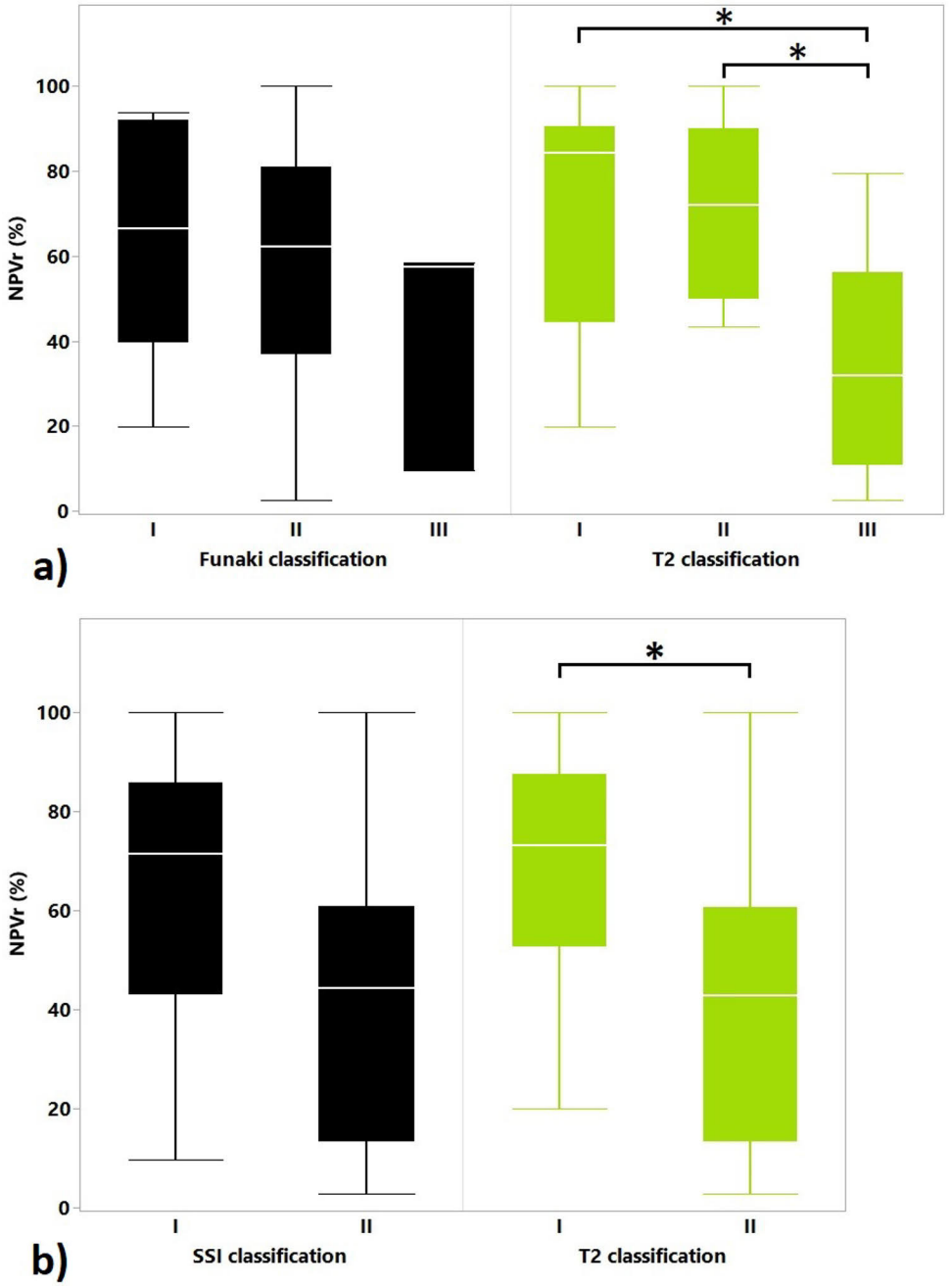

Figure 12. Box-Wisker plots presenting the NPVr (%) for a) the Funaki classification and the T2 classification groups, and b) the SSI classification and the T2 classification groups where an asterisk represents a p-value < 0.05. Modified from study III.

6 Discussion

6.1 The effect of oxytocin on the blood flow

In study I, the effects of oxytocin infusion on the blood flow of different types of uterine fibroids and surrounding tissues were evaluated by comparing the blood flow values to the baseline values using the quantitative DCE-MRI technique. The oxytocin infusion decreased the blood flow of the uterine fibroids in a statistically significant manner without affecting the blood flow of the myometrium which supports the findings of a previous study in which oxytocin infusion decreased the blood flow related parameter values in uterine fibroids while not affecting the values of the uterine wall (Wang et al., 2016). These results seem to indicate that the oxytocin effect takes place in the uterine fibroid, not in the myometrium. However, the underlying mechanism of how the oxytocin infusion decreases the blood flow of uterine fibroids at the histopathological level is still unknown. The mechanism may be related to the amount and location of oxytocin receptors that have been found in the uterine fibroids, the myometrium, and the blood vessels (Lee et al., 1998; Rosseland et al., 2013; Sendemir et al., 2008). Therefore, further investigations of oxytocin receptors are needed to clarify the underlying mechanism.

The skeletal muscle was chosen here as a negative control due to its constant blood flow levels at rest. However, oxytocin infusion caused a statistically significant increase in the blood flow of skeletal muscle which could be explained by a systemic vasodilatative effect of oxytocin which has been reported previously (Rosseland et al., 2013).

The oxytocin infusion decreased the blood flow of all uterine fibroids present in the study regardless of the Funaki type. However, Funaki type I uterine fibroids were not present in this study, and therefore, further studies are needed to investigate if the effect of oxytocin infusion on the blood flow of the uterine fibroids is dependent on the Funaki type.

One limitation of this study was possibly the biased study population due to the selection of the uterine fibroid group; this consisted of patients screened for MRgHIFU treatment which may not represent the general uterine fibroid population. Secondly, the study population was small, and therefore, it was not possible to assess the influence of the location, the classification, and the size of the uterine fibroid on

the response of oxytocin. However, a retrospective power analysis revealed that a sufficient number of patients had been included in the fibroid group to assess the effect of oxytocin infusion on the uterine fibroids. Further studies with larger study groups would be beneficial in evaluating the influence of these factors in the response to oxytocin infusion. Furthermore, the effect of the dosage of oxytocin remains to be investigated in future studies, i.e. whether an increase in the dosage of oxytocin enhances the decrease of the blood flow of the uterine fibroid.

There are also limitations regarding the DCE-MRI technique utilized in this study. The T1 relaxation time mapping method could not be validated due to inaccuracies in the manufactured T1 relaxation time phantoms or in the T1 relaxation time mapping techniques. In the phantom studies, variable flip angle (VFA) and spin echo inversion recovery (RLSQ method) techniques were evaluated with the RLSQ method produced more consistent and accurate measures than the VFA technique. However, the measured T1 relaxation time values did not correspond to the expected values of the manufactured T1 relaxation phantoms. Due to the lack of a literature T1 relaxation value of uterine fibroids, the IR technique for T1 relaxation time mapping was utilized in order to perform the DCE-MRI analysis. The same T1 relaxation time value was used in analyzing both baseline and oxytocin infusion perfusion conditions for each fibroid. Therefore, the change in the blood flow values should not be affected but in the terms of absolute blood flow values, there might be some inaccuracies present. However, the blood flow values of the uterine fibroids in this study were similar as compared to a previous study (Wei et al., 2017).

6.2 Developing quantitative prediction methods for the technical outcome of the MRgHIFU treatment

In study II, the feasibility of apparent diffusion coefficient in predicting the technical outcome of the MRgHIFU treatment of the uterine fibroids was investigated and compared with the existing evaluation method: Funaki classification. The results of the median ADC values of uterine fibroids as calculated with different b-value combinations may suggest that there is a non-mono-exponential dependence between the signal intensity and the b-values. Our results seem to support the hypothesis that DWI can reflect both perfusion and diffusion effects in uterine fibroids as described in a previous study (Ikink et al., 2014).

All other pretreatment MRI parameters correlated with the NPVr except the ADC values calculated with the lowest b-values, suggesting that these other parameters could be good predictors of the MRgHIFU treatment outcomes. However, the lack of statistically significant correlation between the ADC values

calculated with the lowest b-values can be a consequence of the small sample size and the small number of the lowest b-values used in this study. By acquiring larger number of low b-values could have made it possible to determine ADC values with greater accuracy. The ADC values with the lowest b-values could provide information about perfusion without the need for a contrast agent or the rather challenging analysis of quantitative dynamic contrast-enhanced imaging data and therefore, further investigations may be needed.

A new definition of heating efficiency (the total volume of 240 CEM43 contours divided by the total delivered acoustic energy at the focus) was presented in this study which could hypothetically be a more accurate definition for heating efficiency because it is not dependent on user-chosen treatment parameters or the patient's anatomy. However, in this study, the new heating efficiency parameter correlated only with rT2(fibroid/muscle). This may be due to the study's small sample size. Nevertheless, it may warrant further investigation due to the theoretically more accurate heating efficiency values compared to the currently used definition.

The linear regression analysis of the new heating efficiency (total volume of 240 CEM43 contours as a function of the total delivered acoustic energy at the focus) for the Funaki classification and the ADC classification revealed a statistically significant regression effect for Funaki I, Funaki II, ADC I and ADC II classification groups. This may indicate that fibroids in different classification groups have different heating efficiencies (mL/J); for example, ADC I type fibroids have a better heating efficiency than ADC II type fibroids. However, this hypothesis needs to be confirmed in further investigations due to the small sample size in the ADC III and Funaki III classification groups.

The ROC curve analysis for the ADC classification and Funaki classification by NPV ratios showed that the ADC classification had higher sensitivity, specificity, and AUC values for each group. The classifications were then tested with the Chi-square test which revealed that only the ADC classification was a statistically significant predictor of the NPVr. This result supports our hypothesis that a quantitative method could be more reliable in predicting the treatment outcome. However, further research will be needed to confirm these results.

One important limitation of this study was the small total sample size and the small number of Funaki type III and ADC type III fibroids since Funaki type III fibroids are usually excluded in the patient selection process and are not treated with MRgHIFU. The total number of subjects could not be increased due to the use of oxytocin infusion during MRgHIFU treatment which has been shown to increase the treatment efficacy and decrease the blood flow to the fibroid (Lozinski et al., 2018; Wang et al., 2016). Therefore, oxytocin infusion during the MRgHIFU treatment would therefore interfere with the interpretation of the results and patients treated after the completion of this study could not be included. However, even with this

small data set, the ADC classification was better in predicting the NPVr than its Funaki counterpart, suggesting that the ADC classification can be useful in patient selection for MRgHIFU treatment of uterine fibroids. A recently published study also supports our findings; Verpalen et al. showed that a DWI-based quantitative method could be more sensitive in discriminating different fibroid types than the Funaki classification before the MRgHIFU treatment (Verpalen et al., 2020). Another limitation was due to variations in the screening MRI which may have affected the determination of the Funaki classification and the ROC curve results of the Funaki classification. Previous studies have shown that fibroid volume correlates with NPVr which may be an additional factor affecting the ADC classification and the interpretation of the results (Mindjuk et al., 2014; Suomi et al., 2019). Nonetheless, there were no statistically significant differences in the median fibroid volumes between the classification groups suggesting that fibroid volume was not a significant factor here.

Certain aspects need to be taken into account regarding the DWI technique utilized in this study. Careful attention should be paid to diffusion-weighted imaging parameters when the ADC cut-off values are used, because DWI sequence parameters, for example, repetition time, echo time, and choice of b-values can exert an impact on the calculated ADC values (Celik, 2016). On the other hand, ADC values have been shown not to depend on the MR's field strength under fixed imaging parameters (Donati et al., 2013; Eghtedari et al., 2016; Merhemic et al., 2018; Ogura et al., 2015).

In study III, the feasibility of utilizing T2 relaxation time in predicting the technical outcome of MRgHIFU treatment of uterine fibroids was investigated and compared with the existing evaluation methods: Funaki and SSI classifications. The T2 relaxation time validation measurement results of this study indicated that T2 relaxation time maps can be reliably measured from uterine fibroids using a multi-echo fast imaging-based sequence and calculated with the scanner's software (Philips) regardless of the coil setup.

The T2 relaxation time, the T2W signal intensity ratios and the scaled signal intensity (SSI) values all showed statistically significant negative correlations with the NPV ratios. The statistically significant negative correlation between the T2W signal intensity ratios and NPV ratios as well as the correlation between the SSI values and NPV ratios have been reported in previous studies which supports the findings emerging from this study (Park et al., 2015; Sainio et al., 2021). These results indicate that lower T2W signal intensity and the shorter T2 relaxation time of the uterine fibroid before treatment could be good predictors of the technical outcome of the MRgHIFU treatment.

The T2 relaxation time was compared to the Funaki classification and the SSI classification by dividing the T2 relaxation time classification into three and two

groups, respectively. In both cases, the ROC curve analysis showed that the T2 relaxation time classification had higher sensitivity and specificity as well as higher AUC values for each group when compared to the Funaki and the SSI classification groups. The Chi-square test of the classifications revealed that only the T2 relaxation time classifications were statistically significant predictors of the NPVr. These results support the working hypothesis of this study i.e. that a quantitative method could be more reliable in predicting the treatment outcome, a conclusion reported in a previous study using another quantitative method (Sainio et al., 2021).

The limitations of this study were the same as in study II. However, there are also limitations regarding the T2 relaxation time mapping method. The T2 relaxation time mapping is not yet commonly used in clinical routine due to the need for substantial expertise in image acquisition and post-processing. However, we have demonstrated that a multi-echo fast imaging-based technique could be used reliably for T2 relaxation time image acquisition and scanner software can be exploited reliably for calculating the T2 relaxation time maps, which significantly accelerates the imaging and analysis processes. Careful attention should be paid to T2 relaxation time mapping sequence parameters when the T2 relaxation time cut-off values are used, because the sequence parameters, for example, repetition time, and choice of echo times can exert an impact on the calculated T2 relaxation time values (McRobbie et al., 2017).

6.3 Future considerations

Oxytocin infusion during the MRgHIFU treatment of the uterine fibroids is rapidly becoming a part of the clinical routine due to the treatment's increased efficacy. Therefore, further research elucidating the effect of oxytocin infusion on the patient selection process needs to be conducted in larger trials. The precise mechanisms through which oxytocin alters blood flow are still unclear and therefore, further investigations are needed e.g. to examine if there are oxytocin receptors in uterine fibroids and myometrium.

Larger trials are also needed to validate the quantitative MRI classifications created in this thesis. Further research is needed to clarify the feature selection methods including quantitative MRI parameters and clinical patient data for the MRgHIFU treatment outcome classification of the uterine fibroids, including the effect of oxytocin infusion on these features and patient eligibility. Deep learning algorithms could also be used for the MRgHIFU treatment outcome prediction of the uterine fibroids. For example, these could be more accurate in the patient selection process by taking into account the clinical patient data and the uterine fibroid characteristics by incorporating information from the quantitative MRI data.

Other quantitative MRI parameters of uterine fibroids such as intravoxel incoherent motion-related parameters, biexponential modelling of the relaxation times as well as other relaxation time methods (continuous-wave $T_{1\rho}$, adiabatic $T_{1\rho}$, adiabatic $T_{2\rho}$, and relaxation along a fictitious field) could provide novel information about the tissue characteristics of uterine fibroid. Therefore, further investigations are still needed to enable a quantitative MRI of uterine fibroids.

The use of MRgHIFU treatment will become widespread as the technology further improves and new research results are published on patient selection, treatment efficacy, and long-term effects. Perhaps, ultimately, the MRgHIFU treatment will become a major treatment option not only for the uterine fibroids but also for other solid tumours such as bone metastasses. However, there are still major limiting factors such as lack of consistent reimbursement and coverage provided by the insurance companies for MRgHIFU treatment worldwide.

Quantitative MRI has the potential to become more commonly used in clinical routine for tissue characterization, identification of biological changes in diseases, and the assessment of treatment response as the MRI techniques improve and the analysis programs become more user-friendly and automatized, for example by incorporating artificial intelligence.

7 Conclusions

The following conclusions emerge from the results of the studies presented in this thesis:

I. An oxytocin infusion significantly reduces the blood flow of different types of uterine fibroids without an effect on the myometrial blood flow, indicating that the oxytocin effect takes place in the uterine fibroid, not in the myometrium.

II. The apparent diffusion coefficient values are feasible in predicting the technical outcome of MRgHIFU treatment of uterine fibroids and may even outperform the Funaki classification.

III. The T2 relaxation time values are feasible in predicting the technical outcome of MRgHIFU treatment of uterine fibroids, and may well outperform the Funaki and the SSI classifications.

Acknowledgements

This study was carried out at the Department of Radiology and the Department of Medical Physics at Turku University Hospital and the University of Turku during the years 2017-2021. It was financially supported by grants from the Finnish Cultural Foundation, The Varsinais-Suomi Regional Fund of the Finnish Cultural Foundation, the TYKS foundation, the Instrumentarium Science Foundation, the State Research Funding of the Turku Univesity Hospital, the Inkeri and Mauri Vänskä's Foundation, the Paulo Foundation, and the K. Albin Johansson's foundation.

First of all, I wish to express my sincere appreciation to my supervisors, Professor Roberto Blanco Sequeiros and Docent Jani Saunavaara, who have guided and encouraged me through these years with their outstanding intelligence and compassion. It has been a great privilege to have you two as my supervisors. Your great passion for research and your belief in me as a researcher have encouraged me to create an endless desire for doing research. I am also grateful to Roberto Blanco Sequeiros, the Head of Radiology Department, for providing excellent and pioneering facilities for my research, and to Jani Saunavaara, the Assistant Chief Physicist, for guiding me into the fascinating MRI world.

I wish to thank the official reviewers, Professor Seppo Koskinen and Associate Professor Mikko Nissi for giving their valuable time and effort to review this thesis. Your constructive feedback and detailed review have tremendously improved the quality of this thesis.

I would like to thank the follow-up committee, Professor Mika Teräs and Professor Riitta Parkkola, for your valuable support and guidance during my doctoral training.

I am deeply grateful to all my co-authors for their insightful comments and enormous contribution to my manuscripts and research ideas. It has been a great privilege to work with such active and enthusiastic researchers. I wait eagerly for our future studies and publications. I would like to thank radiologist Gaber Komar for the guidance in radiology and generous overall support during these years. The gynaecologists Antti Perheentupa, Kirsi Joronen, and Saara Otonkoski are greatly appreciated for their contribution and requirement of patients. I warmly thank Antti

Viitala for his valuable comments and expertise in the HIFU field. I wish to thank also Sami Mattila for helping with the image analysis.

My greatest appreciation goes to the really skilful MR technologists in the TG3 MRI, Mira Hallenberg, Fanny Nyroos, Kari Jarkko, Viivi Magerholm, Satu Holmström, Kaisa Saarinen, Säde Korpinen, Miia Airola, Anni Koskinen, Ville Roppola, Jouni Nyroos and Iina Luoma-Aho. I wish to express my deepest gratitude also to the whole HIFU team, it has been wonderful to work with you all and to create something new together. The HIFU team is like my second family.

I would like to pay my special regards to my colleagues and coworkers who have encouraged and pushed me through these years. I am grateful for all the insightful conversations I have had with you during this time. Particularly with Ekaterina Saukko, you have indeed encouraged me through these last steps, thank you. I have been so grateful for having such wonderful coworkers and colleagues around me and I cannot thank you enough.

I express my gratitude also to the Laboratory of Industrial Physics where my journey began. I would like to thank Professor Jarno Salonen, the Head of the Laboratory, for fulfilling my naive wish when I asked for a Bachelor thesis topic that will give me reputation and honour. I want to thank also all fellow physicists at the laboratory, especially Outi Alanen and Janne Peltonen for being such wonderful friends to me and always believing in me.

Special thanks also to all my dear friends who have made my life happier and easier over these years. Particularly I am grateful for Kia Tammi who has been my best friend for almost two decades. You have always been there for me when I needed. I would like to appreciate my dear friend Mira Hallenberg especially for our great and joyful journeys together. I want to thank also all my samba friends and Samba Carioca ry for providing a good counterbalance for work and doctoral training, like the slogan says “Samba Yes! Work No!”.

I want to express my deepest gratitude to my parents, Jorma Sainio and Sirpa Sainio, who have supported and encouraged me to study during all these years. I start to think that my passion to study has begun already at a very young age even though it didn’t always feel like that. I warmly thank my sister Tanja Lehti and nephews Jami and Jyri who have brought so much joy to my life.

Most importantly, dear Markus, my husband and best friend – thank you from the bottom of my heart that you have been next to me through these years. You have always believed in me even when I didn’t. You make me so much stronger.

Nousiainen, October 2021
Teija Sainio

References

Al Hilli, M., & Stewart, E. (2010). Magnetic Resonance-Guided Focused Ultrasound Surgery. *Seminars in Reproductive Medicine*, *28*(03), 242–249. https://doi.org/10.1055/s-0030-1251481

Andrews, S., Yuan, Q., Bailey, A., Xi, Y., Chopra, R., Staruch, R., & Pedrosa, I. (2019). Multiparametric MRI Characterization of Funaki Types of Uterine Fibroids Considered for MR-Guided High-Intensity Focused Ultrasound (MR-HIFU) Therapy. *Academic Radiology*, *26*(4), e9–e17. https://doi.org/10.1016/j.acra.2018.05.012

Babsky, A. M., Ju, S., & Bansal, N. (2011). Evaluation of tumor treatment response with diffusion-weighted MRI. In B. Taouli (Ed.), *Extra-Cranial Applications of Diffusion-Weighted MRI* (pp. 172–197). Cambridge University Press. https://doi.org/10.1017/cbo9780511778070.013

Barrera, C. A., Otero, H. J., Hartung, H. D., Biko, D. M., & Serai, S. D. (2019). Protocol optimization for cardiac and liver iron content assessment using MRI: What sequence should I use? *Clinical Imaging*, *56*(December 2018), 52–57. https://doi.org/10.1016/j.clinimag.2019.02.012

Bojorquez, J. Z., Bricq, S., Acquitter, C., Brunotte, F., Walker, P. M., & Lalande, A. (2017). What are normal relaxation times of tissues at 3 T? *Magnetic Resonance Imaging*, *35*, 69–80. https://doi.org/10.1016/j.mri.2016.08.021

Bojorquez, J. Z., Jodoin, P. M., Bricq, S., Walker, P. M., Brunotte, F., & Lalande, A. (2019). Automatic classification of tissues on pelvic MRI based on relaxation times and support vector machine. *PLoS ONE*, *14*(2), 1–17. https://doi.org/10.1371/journal.pone.0211944

Boto, J., Fitsiori, A., Drake-Pérez, M., Vargas, M. I., & Lovblad, K. (2018). Clinical applications of diffusion weighted imaging in neuroradiology. *Insights into Imaging*, *9*(4), 535–547. https://doi.org/10.1007/s13244-018-0624-3

Brace, C. (2011). Thermal Tumor Ablation in Clinical Use. *IEEE Pulse*, *2*(5), 28–38. https://doi.org/10.1109/MPUL.2011.942603

Brown, R. W., Cheng, Y.-. N., Haacke, E. M., Thompson, M. R., Venkatesan, R., & Cheng, Y.-. N. (2014). Chapter 1 Magnetic Resonance Imaging : A Preview. In *Magnetic resonance imaging : physical principles and sequence design*.

Carr, H. Y., & Purcell, E. M. (1954). Effects of diffusion on free precession in nuclear magnetic resonance experiments. *Physical Review*, *94*(3), 630–638. https://doi.org/10.1103/PhysRev.94.630

Celik, A. (2016). Effect of imaging parameters on the accuracy of apparent diffusion coefficient and optimization strategies. *Diagnostic and Interventional Radiology*, *22*(1), 101–107. https://doi.org/10.5152/dir.2015.14440

Chen, H., Li, F., Zhao, X., Yuan, C., Rutt, B., & Kerwin, W. S. (2011). Extended graphical model for analysis of dynamic contrast-enhanced MRI. *Magnetic Resonance in Medicine*, *66*(3), 868–878. https://doi.org/10.1002/mrm.22819

Chu, K. F., & Dupuy, D. E. (2014). Thermal ablation of tumours: Biological mechanisms and advances in therapy. *Nature Reviews Cancer*, *14*(3), 199–208. https://doi.org/10.1038/nrc3672

Cramer, S. F., & Patel, A. (1990). The frequency of uterine leiomyomas. *American Journal of Clinical Pathology*, *94*(4 SUPPL. 1), 435–438.

Cuenod, C. A., & Balvay, D. (2013). Perfusion and vascular permeability: Basic concepts and measurement in DCE-CT and DCE-MRI. *Diagnostic and Interventional Imaging*, *94*(12), 1187–1204. https://doi.org/10.1016/j.diii.2013.10.010

Damadian, R. (1971). Tumor detection by nuclear magnetic resonance. *Science*, *171*(3976), 1151–1153. https://doi.org/10.1126/science.171.3976.1151

Damianou, C. A., Hynynen, K., & Fan, X. (1995). Evaluation of Accuracy of a Theoretical Model for Predicting the Necrosed Tissue Volume during Focused Ultrasound Surgery. *IEEE Transactions on Ultrasonics, Ferroelectrics and Frequency Control*, *42*(2), 182–187. https://doi.org/10.1109/58.365232

Damianou, C. A., & Hynynen, K. H. (1994). The effect of various physical parameters on the size and shape of necrosed tissue volume during ultrasound surgery. *Journal of the Acoustical Society of America*, *95*(3), 1641–1649. https://doi.org/10.1121/1.408550

De Senneville, B. D., Quesson, B., & Moonen, C. T. W. (2005). Magnetic resonance temperature imaging. *International Journal of Hyperthermia*, *21*(6), 515–531. https://doi.org/10.1080/02656730500133785

Donati, O. F., Chong, D., Nanz, D., Boss, A., Froehlich, J. M., Andres, E., Seifert, B., & Thoeny, H. C. (2013). Diffusion-weighted MR Imaging of Upper Abdominal Organs: Field Strength and Intervendor Variability of Apparent Diffusion Coefficients. *Radiology*, *270*(2), 454–463. https://doi.org/10.1148/radiol.13130819

Donnez, J., & Dolmans, M. M. (2016). Uterine fibroid management: From the present to the future. *Human Reproduction Update*, *22*(6), 665–686. https://doi.org/10.1093/humupd/dmw023

Duc, N. M., & Keserci, B. (2018). Review of influential clinical factors in reducing the risk of unsuccessful MRI-guided HIFU treatment outcome of uterine fibroids. *Diagnostic and Interventional Radiology*, *24*(5), 283–291. https://doi.org/10.5152/dir.2018.18111

Eghtedari, M., Ma, J., Fox, P., Guvenc, I., Yang, W. T., & Dogan, B. E. (2016). Effects of magnetic field strength and b value on the sensitivity and specificity of quantitative breast diffusion-weighted MRI. *Quantitative Imaging in Medicine and Surgery*, *6*(4), 374–380. https://doi.org/10.21037/qims.2016.07.06

Ellens, N., & Hynynen, K. (2014). Simulation study of the effects of near- and far-field heating during focused ultrasound uterine fibroid ablation using an electronically focused phased array: A theoretical analysis of patient safety. *Medical Physics*, *41*(7), 1–15. https://doi.org/10.1118/1.4883777

Fennessy, F. M., Tempany, C. M., McDannold, N. J., So, M. J., Hesley, G., Gostout, B., Kim, H. S., Holland, G. A., Sarti, D. A., Hynynen, K., Jolesz, F. A., & Stewart, E. A. (2007). Uterine Leiomyomas: MR Imaging–guided Focused Ultrasound Surgery—Results of Different Treatment Protocols 1 . *Radiology*, *243*(3), 885–893. https://doi.org/10.1148/radiol.2433060267

Fernández-Jiménez, R., Sánchez-González, J., Aguero, J., del Trigo, M., Galán-Arriola, C., Fuster, V., & Ibáñez, B. (2015). Fast T2 gradient-spin-echo (T2-GraSE) mapping for myocardial edema quantification: first in vivo validation in a porcine model of ischemia/reperfusion. *Journal of Cardiovascular Magnetic Resonance*, *17*(1), 92. https://doi.org/10.1186/s12968-015-0199-9

Feuerlein, S., Pauls, S., Juchems, M. S., Stuber, T., Hoffmann, M. H. K., Brambs, H.-J., & Ernst, A. S. (2009). Pitfalls in Abdominal Diffusion-Weighted Imaging: How Predictive is Restricted Water Diffusion for Malignancy. *American Journal of Roentgenology*, *193*(4), 1070–1076. https://doi.org/10.2214/AJR.08.2093

Funaki, K., Fukunishi, H., Funaki, T., Sawada, K., Kaji, Y., & Maruo, T. (2007). Magnetic resonance-guided focused ultrasound surgery for uterine fibroids: relationship between the therapeutic effects and signal intensity of preexisting T2-weighted magnetic resonance images. *American Journal of Obstetrics and Gynecology*, *196*(2), 1–6. https://doi.org/10.1016/j.ajog.2006.08.030

Funaki, K., Fukunishi, H., & Sawada, K. (2009). Clinical outcomes of magnetic resonance-guided focused ultrasound surgery for uterine myomas: 24-Month follow-up. *Ultrasound in Obstetrics and Gynecology*, *34*(5), 584–589. https://doi.org/10.1002/uog.7455

Goldberg, S. N., Grassi, C. J., Cardella, J. F., Charboneau, J. W., Dodd, G. D., Dupuy, D. E., Gervais, D., Gillams, A. R., Kane, R. A., Lee, F. T., Livraghi, T., McGahan, J., Phillips, D. A., Rhim, H., & Silverman, S. G. (2005). Image-guided Tumor Ablation: Standardization of Terminology and Reporting Criteria. *Radiology*, *235*(3), 728–739. https://doi.org/10.1148/radiol.2353042205

Gracien, R. M., Maiworm, M., Brüche, N., Shrestha, M., Nöth, U., Hattingen, E., Wagner, M., & Deichmann, R. (2020). How stable is quantitative MRI? – Assessment of intra- and inter-scanner-model reproducibility using identical acquisition sequences and data analysis programs. *NeuroImage*, *207*(November 2019), 1–11. https://doi.org/10.1016/j.neuroimage.2019.116364

Gulani, V., & Seiberlich, N. (2020). *Quantitative MRI: Rationale and Challenges*. xxxvii–li. https://doi.org/10.1016/b978-0-12-817057-1.00001-9

Hadizadeh, D. R., Mädler, B., Gieseke, J., Fimmers, R., Hattingen, E., & Schild, H. H. (2017). Effects of arterial input function selection on kinetic parameters in brain dynamic contrast-enhanced MRI. *Magnetic Resonance Imaging*, *40*, 83–90. https://doi.org/10.1016/j.mri.2017.04.006

Hänninen, N., Rautiainen, J., Rieppo, L., Saarakkala, S., & Nissi, M. J. (2017). Orientation anisotropy of quantitative MRI relaxation parameters in ordered tissue. *Scientific Reports*, *7*(1), 9606. https://doi.org/10.1038/s41598-017-10053-2

Hardy, P. A., Henkelman, R. M., Bishop, J. E., Poon, E. C. S., & Plewes, D. B. (1992). Why fat is bright in rare and fast spin-echo imaging. *Journal of Magnetic Resonance Imaging*, *2*(5), 533–540. https://doi.org/10.1002/jmri.1880020511

Havryliuk, Y., Setton, R., Carlow, J. J., & Shaktman, B. D. (2017). Symptomatic Fibroid Management: Systematic Review of the Literature. *JSLS : Journal of the Society of Laparoendoscopic Surgeons*, *21*(3). https://doi.org/10.4293/JSLS.2017.00041

Hesley, G. K., Gorny, K. R., Henrichsen, T. L., Woodrum, D. A., & Brown, D. L. (2008). A clinical review of focused ultrasound ablation with magnetic resonance guidance: An option for treating uterine fibroids. *Ultrasound Quarterly*, *24*(2), 131–139. https://doi.org/10.1097/RUQ.0b013e31817c5e0c

Hesley, G. K., Gorny, K. R., & Woodrum, D. A. (2013). MR-Guided Focused Ultrasound for the Treatment of Uterine Fibroids. *CardioVascular and Interventional Radiology*, *36*(1), 5–13. https://doi.org/10.1007/s00270-012-0367-3

Hill, C. R., Bamber, J. C., & ter Haar, G. R. (2004). *Physical Principles of Medical Ultrasonics* (Second edi). John Wiley & Sons, Ltd.

Hindley, J., Regan, L., Stewart, E., Tempany, C., Hynnen, K., Inbar, Y., Kim, K., Geschwind, J., Hesley, G., Gostout, B., & Sklair-Levy, M. (2004). MRI guidance of focused ultrasound therapy of uterine fibroids: early results. *American Journal of Roentgenology*, *183*(December), 1713–1719.

Hocquelet, A., Denis de Senneville, B., Frulio, N., Salut, C., Bouzgarrou, M., Papadopoulos, P., & Trillaud, H. (2017). Magnetic resonance texture parameters are associated with ablation efficiency in MR-guided high-intensity focussed ultrasound treatment of uterine fibroids. *International Journal of Hyperthermia*, *33*(2), 142–149. https://doi.org/10.1080/02656736.2016.1241432

Holdsworth-Carson, S. J., Zhao, D., Cann, L., Bittinger, S., Nowell, C. J., & Rogers, P. A. W. (2016). Differences in the cellular composition of small versus large uterine fibroids. *Reproduction*, *152*(5), 467–480. https://doi.org/10.1530/REP-16-0216

Ikink, M. E., Voogt, M. J., Van Den Bosch, M. A. A. J., Nijenhuis, R. J., Keserci, B., Kim, Y. S., Vincken, K. L., & Bartels, L. W. (2014). Diffusion-weighted magnetic resonance imaging using different b-value combinations for the evaluation of treatment results after volumetric MR-guided high-intensity focused ultrasound ablation of uterine fibroids. *European Radiology*, *24*(9), 2118–2127. https://doi.org/10.1007/s00330-014-3274-y

in den Kleef, J. J. E., & Cuppen, J. J. M. (1987). RLSQ:T1,T2, and ρ calculations, combining ratios and least squares. *Magnetic Resonance in Medicine*, *5*(6), 513–524. https://doi.org/10.1002/mrm.1910050602

Jackson, A., Buckley, D. L., & Parker, G. J. M. (2005). Dynamic Contrast-Enhanced Magnetic Resonance Imaging in Oncology. In A. Jackson, D. L. Buckley, & G. J. M. Parker (Eds.), *Springer*

Berlin Heidelberg New York (Vol. 53, Issue 9). Springer Berlin Heidelberg. https://doi.org/10.1007/b137553

Jacobs, M. A., Gultekin, D. H., & Kim, H. S. (2010). Comparison between diffusion-weighted imaging, T2-weighted, and postcontrast T1-weighted imaging after MR-guided, high intensity, focused ultrasound treatment of uterine leiomyomata: preliminary results. *Medical Physics*, *37*(9), 4768–4776. https://doi.org/10.1118/1.3475940

Jambor, I., Verho, J., Ettala, O., Knaapila, J., Taimen, P., Syvänen, K. T., Kiviniemi, A., Kähkönen, E., Perez, I. M., Seppänen, M., Rannikko, A., Oksanen, O., Riikonen, J., Vimpeli, S. M., Kauko, T., Merisaari, H., Kallajoki, M., Mirtti, T., Lamminen, T., … Boström, P. J. (2019). Validation of improd biparametric mri in men with clinically suspected prostate cancer: A prospective multi-institutional trial. *PLoS Medicine*, *16*(6), 1–14. https://doi.org/10.1371/journal.pmed.1002813

Jayes, F. L., Liu, B., Feng, L., Aviles-Espinoza, N., Leikin, S., & Leppert, P. C. (2019). Evidence of biomechanical and collagen heterogeneity in uterine fibroids. *PLoS ONE*, *14*(4), 1–16. https://doi.org/10.1371/journal.pone.0215646

Jenne, J. W., Preusser, T., & Günther, M. (2012). High-intensity focused ultrasound: Principles, therapy guidance, simulations and applications. *Zeitschrift Fur Medizinische Physik*, *22*(4), 311–322. https://doi.org/10.1016/j.zemedi.2012.07.001

Jolesz, F. A. (2009). MRI-guided focused ultrasound surgery. *Annual Review of Medicine*, *60*(9), 417–430. https://doi.org/10.1146/annurev.med.60.041707.170303

Jolesz, F. A., & Hynynen, K. (2007). *MRI-Guided Focused Ultrasound Surgery* (F. A. Jolesz & K. Hynynen (eds.)). CRC Press.

Kele, P. G. (2010). Diffusion weighted imaging in the liver. *World Journal of Gastroenterology*, *16*(13), 1567. https://doi.org/10.3748/wjg.v16.i13.1567

Keserci, B., & Duc, N. M. (2018). Magnetic Resonance Imaging Parameters in Predicting the Treatment Outcome of High-intensity Focused Ultrasound Ablation of Uterine Fibroids With an Immediate Nonperfused Volume Ratio of at Least 90%. *Academic Radiology*, 1–13. https://doi.org/10.1016/j.acra.2018.01.022

Khalifa, F., Soliman, A., El-baz, A., El-ghar, M. A., El-diasty, T., Gimel, G., Ouseph, R., Dwyer, A. C., & Khalifa, F. (2016). Models and methods for analyzing DCE-MRI : A review. *The International Journal of Medical Physics Research and Practice*, *124301*(2014). https://doi.org/10.1118/1.4898202

Khan, A. T., Shehmar, M., & Gupta, J. K. (2014). Uterine fibroids: Current perspectives. *International Journal of Women's Health*, *6*(1), 95–114. https://doi.org/10.2147/IJWH.S51083

Kim, Y.-S. (2015). Advances in MR image-guided high-intensity focused ultrasound therapy. *International Journal of Hyperthermia*, *31*(3), 225–232. https://doi.org/10.3109/02656736.2014.976773

Kim, Y.-S., Bae, D. S., Park, M. J., Viitala, A., Keserci, B., Rhim, H., & Lim, H. K. (2014). Techniques to expand patient selection for MRI-guided high-intensity focused ultrasound ablation of uterine fibroids. *American Journal of Roentgenology*, *202*(2), 443–451. https://doi.org/10.2214/AJR.13.10753

Kim, Y.-S., Keserci, B., Partanen, A., Rhim, H., Lim, H. K., Park, M. J., & Köhler, M. O. (2012). Volumetric MR-HIFU ablation of uterine fibroids: Role of treatment cell size in the improvement of energy efficiency. *European Journal of Radiology*, *81*(11), 3652–3659. https://doi.org/10.1016/j.ejrad.2011.09.005

Kim, Y.-S., Kim, B.-G., Rhim, H., Bae, D.-S., Lee, J.-W., Kim, T.-J., Choi, C. H., Lee, Y.-Y., & Lim, H. K. (2014). Uterine fibroids: semiquantitative perfusion MR imaging parameters associated with the intraprocedural and immediate postprocedural treatment efficiencies of MR imaging-guided high-intensity focused ultrasound ablation. *Radiology*, *273*(2), 462–471. https://doi.org/10.1148/radiol.14132719

Kim, Y.-S., Kim, J.-H., Rhim, H., Lim, H. K., Keserci, B., Bae, D.-S., Kim, B.-G., Lee, J.-W., Kim, T.-J., & Choi, C. H. (2012). High-Intensity Focused Ultrasound Ablation with a One-Layer Strategy

to Treat Large Uterine Fibroids : Initial Clinical Outcomes. *Radiology*, *263*(2). https://doi.org/10.1148/radiol.12111707/-/DC1

Kim, Y.-S., Lee, J.-W., Choi, C. H., Kim, B.-G., Bae, D.-S., Rhim, H., & Lim, H. K. (2016). Uterine Fibroids: Correlation of T2 Signal Intensity with Semiquantitative Perfusion MR Parameters in Patients Screened for MR-guided High-Intensity Focused Ultrasound Ablation. *Radiology*, *278*(3), 925–935. https://doi.org/10.1148/radiol.2015150608

Kim, Y.-S., Lim, H. K., Kim, J.-H., Rhim, H., Park, B. K., Keserci, B., Köhler, M. O., Bae, D.-S., Kim, B.-G., Lee, J.-W., Kim, T.-J., Sokka, S., & Lee, J. H. (2011). Dynamic Contrast-Enhanced Magnetic Resonance Imaging Predicts Immediate Therapeutic Response of Magnetic Resonance-Guided High-Intensity Focused Ultrasound Ablation of Symptomatic Uterine Fibroids. *Investigative Radiology*, *46*(10), 639–647. https://doi.org/10.1097/RLI.0b013e318220785c

Kim, Y.-S., Lim, H. K., & Rhim, H. (2016). Magnetic resonance imaging-guided high- intensity focused ultrasound ablation of Uterine Fibroids: Effect of bowel interposition on procedure feasibility and a unique bowel displacement technique. *PLoS ONE*, *11*(5), 1–14. https://doi.org/10.1371/journal.pone.0155670

Kröncke, T., & David, M. (2019). MR-Guided Focused Ultrasound in Fibroid Treatment – Results of the 4th Radiological-Gynecological Expert Meeting. *RöFo - Fortschritte Auf Dem Gebiet Der Röntgenstrahlen Und Der Bildgebenden Verfahren*, *191*(07), 626–629. https://doi.org/10.1055/a-0884-3143

Larsson, C., Kleppestø, M., Grothe, I., Vardal, J., & Bjørnerud, A. (2015). T1 in high-grade glioma and the influence of different measurement strategies on parameter estimations in DCE-MRI. *Journal of Magnetic Resonance Imaging*, *42*(1), 97–104. https://doi.org/10.1002/jmri.24772

Le Bihan, D., Breton, E., Lallemand, D., Aubin, M.-L., Vignaud, J., & Laval-Jeantet, M. (1988). Separation of diffusion and perfusion in intravoxel incoherent motion MR imaging. *Radiology*, *168*(2), 497–505. https://doi.org/10.1148/radiology.168.2.3393671

Lee, K.-H., Khan-Dawood, F. S., & Dawood, M. Y. (1998). Oxytocin receptor and its messenger ribonucleic acid in human leiomyoma and myometrium. *American Journal of Obstetrics and Gynecology*, *179*(3), 620–627. https://doi.org/10.1016/S0002-9378(98)70054-7

Li, C., Jin, C., Liang, T., Li, X., Wang, R., Zhang, Y., & Yang, J. (2020). Magnetic resonance-guided high-intensity focused ultrasound of uterine fibroids: whole-tumor quantitative perfusion for prediction of immediate ablation response. *Acta Radiologica*, *61*(8), 1125–1133. https://doi.org/10.1177/0284185119891692

Liu, J., Keserci, B., Yang, X., Wei, J., Rong, R., Zhu, Y., & Wang, X. (2014). Volume transfer constant (K trans) maps from dynamic contrast enhanced MRI as potential guidance for MR-guided high intensity focused ultrasound treatment of hypervascular uterine fi broids. *Magnetic Resonance Imaging*, *32*(9), 1156–1161. https://doi.org/10.1016/j.mri.2014.05.005

Lozinski, T., Filipowska, J., Krol, P., Kubaty, A., & Wegrzyn, P. (2018). Oxytocin Administration in High-Intensity Focused Ultrasound Treatment of Myomata. *BioMed Research International*, *2018*. https://doi.org/10.1155/2018/7518026

Magalhães Peregrino, P. F., Messina, M. D. L., Simões, R. D. S., Soares-Júnior, J. M., & Baracat, E. C. (2017). Review of magnetic resonance-guided focused ultrasound in the treatment of uterine fibroids. *Clinics*, *72*(10), 637–641. https://doi.org/10.6061/clinics/2017(10)08

Mannelli, L., Nougaret, S., Vargas, H. A., & Do, R. K. G. (2015). Advances in Diffusion-Weighted Imaging. *Radiologic Clinics of North America*, *53*(3), 569–581. https://doi.org/10.1016/j.rcl.2015.01.002

Mars, M., Chelli, M., Tbini, Z., Ladeb, F., & Gharbi, S. (2018). MRI T2 Mapping of Knee Articular Cartilage Using Different Acquisition Sequences and Calculation Methods at 1.5 Tesla. *Medical Principles and Practice*, *27*(5), 443–450. https://doi.org/10.1159/000490796

Matzat, S. J., McWalter, E. J., Kogan, F., Chen, W., & Gold, G. E. (2015). T2 Relaxation time quantitation differs between pulse sequences in articular cartilage. *Journal of Magnetic Resonance Imaging*, *42*(1), 105–113. https://doi.org/10.1002/jmri.24757

McDannold, N. J., King, R. L., Jolesz, F. A., & Hynynen, K. H. (2000). Usefulness of MR Imaging-Derived Thermometry and Dosimetry in Determining the Threshold for Tissue Damage Induced by Thermal Surgery in Rabbits. *Radiology*, *216*(2), 517–523. https://doi.org/10.1148/radiology.216.2.r00au42517

McRobbie, D. W., Moore, E. A., & Graves, M. J. (2017). MRI from picture to proton. In *MRI from Picture to Proton*. https://doi.org/10.2214/ajr.182.3.1820592

Merhemic, Z., Imsirovic, B., Bilalovic, N., Stojanov, D., Boban, J., & Thurnher, M. M. (2018). Apparent diffusion coefficient reproducibility in brain tumors measured on 1.5 and 3 T clinical scanners: A pilot study. *European Journal of Radiology*, *108*(May), 249–253. https://doi.org/10.1016/j.ejrad.2018.10.010

Mikami, K., Murakami, T., Okada, A., Osuga, K., Tomoda, K., & Nakamura, H. (2008). Magnetic resonance imaging-guided focused ultrasound ablation of uterine fibroids: Early clinical experience. *Radiation Medicine - Medical Imaging and Radiation Oncology*, *26*(4), 198–205. https://doi.org/10.1007/s11604-007-0215-6

Mindjuk, I., Trumm, C., Herzog, P., Stahl, R., & Matzko, M. (2014). MRI predictors of clinical success in MR-guided focused ultrasound (MRgFUS) treatments of uterine fibroids: results from a single centre. *European Radiology*, *25*(5), 1317–1328. https://doi.org/10.1007/s00330-014-3538-6

Morani, A. C. (2013). Abdominal applications of diffusion-weighted magnetic resonance imaging: Where do we stand. *World Journal of Radiology*, *5*(3), 68. https://doi.org/10.4329/wjr.v5.i3.68

Mosher, T. J., & Dardzinski, B. J. (2004). Cartilage MRI T2 relaxation time mapping: Overview and applications. *Seminars in Musculoskeletal Radiology*, *8*(4), 355–368. https://doi.org/10.1055/s-2004-861764

Munro, M. G., Critchley, H. O. D., Broder, M. S., & Fraser, I. S. (2011). FIGO classification system (PALM-COEIN) for causes of abnormal uterine bleeding in nongravid women of reproductive age. *International Journal of Gynecology and Obstetrics*, *113*(1), 3–13. https://doi.org/10.1016/j.ijgo.2010.11.011

Nam, J. G., Kang, K. M., Choi, S. H., Lim, W. H., Yoo, R. E., Kim, J. H., Yun, T. J., & Sohn, C. H. (2017). Comparison between the prebolus T1 measurement and the fixed T1 value in dynamic contrast-enhanced MR imaging for the differentiation of true progression from pseudoprogression in glioblastoma treated with concurrent radiation therapy and temozolomide che. *American Journal of Neuroradiology*, *38*(12), 2243–2250. https://doi.org/10.3174/ajnr.A5417

Napoli, A., Alfieri, G., Andrani, F., Scipione, R., Manganaro, L., Pecorini, F., & Catalano, C. (2021). Uterine Myomas: Focused Ultrasound Surgery. *Seminars in Ultrasound, CT and MRI*, *42*(1), 25–36. https://doi.org/10.1053/j.sult.2020.08.001

Nikiforaki, K., Ioannidis, G. S., Lagoudaki, E., Manikis, G. H., de Bree, E., Karantanas, A., Maris, T. G., & Marias, K. (2020). Multiexponential T2 relaxometry of benign and malignant adipocytic tumours. *European Radiology Experimental*, *4*(1). https://doi.org/10.1186/s41747-020-00175-0

Nissi, M. J., Rieppo, J., Töyräs, J., Laasanen, M. S., Kiviranta, I., Jurvelin, J. S., & Nieminen, M. T. (2006). T2 relaxation time mapping reveals age- and species-related diversity of collagen network architecture in articular cartilage. *Osteoarthritis and Cartilage*, *14*(12), 1265–1271. https://doi.org/10.1016/j.joca.2006.06.002

Nöth, U., Shrestha, M., Schüre, J. R., & Deichmann, R. (2017). Quantitative in vivo T2 mapping using fast spin echo techniques – A linear correction procedure. *NeuroImage*, *157*, 476–485. https://doi.org/10.1016/j.neuroimage.2017.06.017

Oguchi, O., Mori, A., Kobayashi, Y., Horiuchi, A., Nikaido, T., & Fujii, S. (1995). Prediction of Histopathologic Features and Proliferative Activity of Uterine Leiomyoma by Magnetic Resonance Imaging Prior to GnRH Analogue Therapy: Correlation between T2-Weighted Images and Effect of GnRH Analogue. *Journal of Obstetrics and Gynaecology*, *21*(2), 107–117. https://doi.org/10.1111/j.1447-0756.1995.tb01083.x

Ogura, A., Tamura, T., Ozaki, M., Doi, T., Fujimoto, K., Miyati, T., Ito, Y., Maeda, F., Tarewaki, H., & Takahashi, M. (2015). Apparent diffusion coefficient value is not dependent on magnetic

resonance systems and field strength under fixed imaging parameters in brain. *Journal of Computer Assisted Tomography*, *39*(5), 760–765. https://doi.org/10.1097/RCT.0000000000000266

Oshio, K., & Feinberg, D. A. (1991). GRASE (Gradient-and Spin-Echo) imaging: A novel fast MRI technique. *Magnetic Resonance in Medicine*, *20*(2), 344–349. https://doi.org/10.1002/mrm.1910200219

Papanikolaou, N., Maniatis, V., Pappas, J., Roussakis, A., Efthimiadou, R., & Andreou, J. (2002). Biexponential T2 relaxation time analysis of the brain: Correlation with magnetization transfer ratio. *Investigative Radiology*, *37*(7), 363–367. https://doi.org/10.1097/00004424-200207000-00001

Park, H., Yoon, S. W., & Sokolov, A. (2015). Scaled signal intensity of uterine fibroids based on T2-weighted MR images: a potential objective method to determine the suitability for magnetic resonance-guided focused ultrasound surgery of uterine fibroids. *European Radiology*, *25*(12), 3455–3458. https://doi.org/10.1007/s00330-015-3806-0

Park, M. J., Kim, Y. S., Rhim, H., & Lim, H. K. (2014). Safety and therapeutic efficacy of complete or near-complete ablation of symptomatic uterine fibroid tumors by MR imaging-guided high-intensity focused US Therapy. *Journal of Vascular and Interventional Radiology*, *25*(2), 231–239. https://doi.org/10.1016/j.jvir.2013.11.011

Parker, W. H. (2007). Uterine myomas: management. *Fertility and Sterility*, *88*(2), 255–271. https://doi.org/10.1016/j.fertnstert.2007.06.044

Patlak, C. S., Blasberg, R. G., & Fenstermacher, J. D. (1983). Graphical Evaluation of Blood-to-Brain Transfer Constants from Multiple-Time Uptake Data. *Journal of Cerebral Blood Flow & Metabolism*, *3*(1), 1–7. https://doi.org/10.1038/jcbfm.1983.1

Pilatou, M. C., Stewart, E. A., Maier, S. E., Fennessy, F. M., Hynynen, K., Tempany, C. M. C., & McDannold, N. (2009). MRI-based thermal dosimetry and diffusion-weighted imaging of MRI-guided focused ultrasound thermal ablation of uterine fibroids. *Journal of Magnetic Resonance Imaging*, *29*(2), 404–411. https://doi.org/10.1002/jmri.21688

Quaia, E., Toffanin, R., Guglielmi, G., Ukmar, M., Rossi, A., Martinelli, B., & Cova, M. A. (2008). Fast T2 mapping of the patellar articular cartilage with gradient and spin-echo magnetic resonance imaging at 1.5 T: validation and initial clinical experience in patients with osteoarthritis. *Skeletal Radiology*, *37*(6), 511–517. https://doi.org/10.1007/s00256-008-0478-8

Raiko, J., Koskensalo, K., & Sainio, T. (2020). Imaging-based internal body temperature measurements: The journal Temperature toolbox. *Temperature*, *7*(4), 363–388. https://doi.org/10.1080/23328940.2020.1769006

Reiter, D. A., Lin, P. C., Fishbein, K. W., & Spencer, R. G. (2009). Multicomponent T2 relaxation analysis in cartilage. *Magnetic Resonance in Medicine*, *61*(4), 803–809. https://doi.org/10.1002/mrm.21926

Rieke, V., & Pauly, K. B. (2008). MR thermometry. *Journal of Magnetic Resonance Imaging*, *27*(2), 376–390. https://doi.org/10.1002/jmri.21265

Rivens, I., Shaw, A., Civale, J., & Morris, H. (2009). *Treatment monitoring and thermometry for therapeutic focused ultrasound*. *6736*. https://doi.org/10.1080/02656730701207842

Rosseland, L. A., Hauge, T. H., Grindheim, G., Stubhaug, A., & Langesæter, E. (2013). Changes in Blood Pressure and Cardiac Output during Cesarean Delivery. *Anesthesiology*, *119*(3), 541–551. https://doi.org/10.1097/ALN.0b013e31829416dd

Rueff, L., & Raman, S. (2013). Clinical and Technical Aspects of MR-Guided High Intensity Focused Ultrasound for Treatment of Symptomatic Uterine Fibroids. *Seminars in Interventional Radiology*, *30*(04), 347–353. https://doi.org/10.1055/s-0033-1359728

Sainio, T., Komar, G., Saunavaara, J., Suomi, V., Joronen, K., Perheentupa, A., Viitala, A., & Sequeiros, R. B. (2018). Wedged gel pad for bowel manipulation during MR-guided high-intensity focused ultrasound therapy to treat uterine fibroids: a case report. *Journal of Therapeutic Ultrasound*, *6*(1), 10. https://doi.org/10.1186/s40349-018-0116-4

Sainio, T., Saunavaara, J., Komar, G., Mattila, S., Otonkoski, S., Joronen, K., Perheentupa, A., & Blanco Sequeiros, R. (2021). Feasibility of apparent diffusion coefficient in predicting the technical outcome of MR-guided high-intensity focused ultrasound treatment of uterine fibroids–a comparison with the Funaki classification. *International Journal of Hyperthermia*, *38*(1), 85–94. https://doi.org/10.1080/02656736.2021.1874545

Samei, E., Peck, D. J., Siewerdsen, J. H., & Ritenour, E. R. (2019). Ultrasonography. In E. Samei, D. J. Peck, J. H. Siewerdsen, & E. R. Ritenour (Eds.), *Hendee's Physics of Medical Imaging* (5th ed., pp. 305–338). John Wiley & Sons Ltd.

Sammet, S. (2016). Magnetic resonance safety. *Abdominal Radiology*, *41*(3), 444–451. https://doi.org/10.1007/s00261-016-0680-4

Sapareto, S. A., & Dewey, W. C. (1984). Thermal dose determination in cancer therapy. *International Journal of Radiation Oncology Biology Physics*, *10*(6), 787–800. https://doi.org/10.1016/0360-3016(84)90379-1

Sbano, H., & Padhani, A. R. (2011). Diffusion-weighted MRI of female pelvic tumors. In B. Taouli (Ed.), *Extra-Cranial Applications of Diffusion-Weighted MRI* (pp. 119–143). Cambridge University Press. https://doi.org/10.1017/cbo9780511778070.010

Seiler, A., Nöth, U., Hok, P., Reiländer, A., Maiworm, M., Baudrexel, S., Meuth, S., Rosenow, F., Steinmetz, H., Wagner, M., Hattingen, E., Deichmann, R., & Gracien, R. M. (2021). Multiparametric Quantitative MRI in Neurological Diseases. *Frontiers in Neurology*, *12*(March). https://doi.org/10.3389/fneur.2021.640239

Sendemir, A., Sendemir, E., Kosmehl, H., & Jirikowski, G. F. (2008). Expression of sex hormone-binding globulin, oxytocin receptor, caveolin-1 and p21 in leiomyoma. *Gynecological Endocrinology*, *24*(2), 105–112. https://doi.org/10.1080/09513590701690274

Serai, S. D. (2021). Basics of magnetic resonance imaging and quantitative parameters T1, T2, T2*, T1rho and diffusion-weighted imaging. *Pediatric Radiology*, *17*(2), 66–82. https://doi.org/10.1007/s00247-021-05042-7

Sharafi, A., Chang, G., & Regatte, R. R. (2017). Bi-component T1ρ and T2 Relaxation Mapping of Skeletal Muscle In-Vivo. *Scientific Reports*, *7*(1), 1–9. https://doi.org/10.1038/s41598-017-14581-9

Sharafi, A., Chang, G., & Regatte, R. R. (2018). Biexponential T 2 relaxation estimation of human knee cartilage in vivo at 3T. *Journal of Magnetic Resonance Imaging*, *47*(3), 809–819. https://doi.org/10.1002/jmri.25778

She, W. H., Cheung, T. T., Jenkins, C. R., & Irwin, M. G. (2016). Clinical applications of high-intensity focused ultrasound. *Hong Kong Medical Journal*, 1–11. https://doi.org/10.12809/hkmj154755

Shimada, K., Ohashi, I., Kasahara, I., Watanabe, H., Ohta, S., Miyasaka, N., Itoh, E., & Shibuya, H. (2004). Differentiation between completely hyalinized uterine leiomyomas and ordinary leiomyomas: Three-phase dynamic magnetic resonance imaging (MRI) vs. diffusion-weighted MRI with very small b-factors. *Journal of Magnetic Resonance Imaging*, *20*(1), 97–104. https://doi.org/10.1002/jmri.20063

Sigmund, E. E., & Jensen, J. (2011). Basic physical principles of body diffusion-weighted MRI. In B. Taouli (Ed.), *Extra-Cranial Applications of Diffusion-Weighted MRI* (pp. 1–17). Cambridge University Press. https://doi.org/10.1017/cbo9780511778070.002

Sourbron, S., Ingrisch, M., Siefert, A., Reiser, M., & Herrmann, K. (2009). Quantification of cerebral blood flow, cerebral blood volume, and blood-brain-barrier leakage with DCE-MRI. *Magnetic Resonance in Medicine*, *62*(1), 205–217. https://doi.org/10.1002/mrm.22005

Sourbron, S. P., & Buckley, D. L. (2012). Tracer kinetic modelling in MRI: Estimating perfusion and capillary permeability. *Physics in Medicine and Biology*, *57*(2). https://doi.org/10.1088/0031-9155/57/2/R1

Sourbron, Steven P., & Buckley, D. L. (2011). On the scope and interpretation of the Tofts models for DCE-MRI. *Magnetic Resonance in Medicine*, *66*(3), 735–745. https://doi.org/10.1002/mrm.22861

Spies, J. B., Coyne, K., Guaou Guaou, N., Boyle, D., & Skyrnarz-Murphy, K. Gonzalves, S. M. (2002). The UFS-QOL, a new disease-specific symptom and health-related quality of life questionnaire for leiomyomata. *Obstetrics & Gynecology*, *99*(2), 290–300. https://doi.org/10.1016/S0029-7844(01)01702-1

Sprinkart, A. M., Luetkens, J. A., Träber, F., Doerner, J., Gieseke, J., Schnackenburg, B., Schmitz, G., Thomas, D., Homsi, R., Block, W., Schild, H., & Naehle, C. P. (2015). Gradient Spin Echo (GraSE) imaging for fast myocardial T2 mapping. *Journal of Cardiovascular Magnetic Resonance*, *17*(1), 12. https://doi.org/10.1186/s12968-015-0127-z

Sridhar, D., & Kohi, M. P. (2018). Updates on MR-Guided Focused Ultrasound for Symptomatic Uterine Fibroids. *Seminars in Interventional Radiology*, *35*(1), 17–22. https://doi.org/10.1055/s-0038-1636516

Srivastava, A., Mehrotra, G., Bhargava, S., Agarwal, S., & Tripathi, R. (2008). Studies on the time course of apparent diffusion coefficient and signal intensities on T2- and diffusion-weighted MR Imaging in acute cerebral ischemic stroke. *Journal of Medical Physics*, *33*(4), 162. https://doi.org/10.4103/0971-6203.44479

Stejskal, E. O., & Tanner, J. E. (1965). Spin Diffusion Measurements : Spin Echoes in the Presence of a Time - Dependent Field Gradient. *The Journal of Chemical Physics*, *42*(1), 288–292. https://doi.org/10.1063/1.1695690

Stewart, E. A. (2001). Uterine fibroids. *Lancet*, *357*(9252), 293–298. https://doi.org/10.1016/S0140-6736(00)03622-9

Stewart, E. A., Gedroyc, W. M. W., Tempany, C. M. C., Quade, B. J., Inbar, Y., Ehrenstein, T., Shushan, A., Hindley, J. T., Goldin, R. D., David, M., Sklair, M., & Rabinovici, J. (2003). Focused ultrasound treatment of uterine fibroid tumors: Safety and feasibility of a noninvasive thermoablative technique. *American Journal of Obstetrics and Gynecology*, *189*(1), 48–54. https://doi.org/10.1067/mob.2003.345

Stewart, E. A., Gostout, B., Rabinovici, J., Kim, H. S., Regan, L., & Tempany, C. M. C. (2007). Sustained Relief of Leiomyoma Symptoms by Using Focused Ultrasound Surgery. *Obstetrics & Gynecology*, *110*(2, Part 1), 279–287. https://doi.org/10.1097/01.AOG.0000275283.39475.f6

Stewart, E. A., Rabinovici, J., Tempany, C. M. C., Inbar, Y., Regan, L., Gastout, B., Hesley, G., Kim, H. S., Hengst, S., & Gedroyc, W. M. W. (2006). Clinical outcomes of focused ultrasound surgery for the treatment of uterine fibroids. *Fertility and Sterility*, *85*(1), 22–29. https://doi.org/10.1016/j.fertnstert.2005.04.072

Suomi, V., Komar, G., Sainio, T., Joronen, K., Perheentupa, A., & Blanco Sequeiros, R. (2019). Comprehensive feature selection for classifying the treatment outcome of high-intensity ultrasound therapy in uterine fibroids. *Scientific Reports*, *9*(1), 1–11. https://doi.org/10.1038/s41598-019-47484-y

Swe, T. T., Onitsuka, H., Kawamoto, K., Ueyama, T., Tsuruchi, N., & Masuda, K. (1992). Uterine leiomyoma: correlation between signal intensity on magnetic resonance imaging and pathologic characteristics. *Radiation Medicine*, *10*(6), 235–242. http://www.ncbi.nlm.nih.gov/pubmed/1287735

Taylor, A. J., Salerno, M., Dharmakumar, R., & Jerosch-Herold, M. (2016). T1 Mapping Basic Techniques and Clinical Applications. *JACC: Cardiovascular Imaging*, *9*(1), 67–81. https://doi.org/10.1016/j.jcmg.2015.11.005

Tempany, C. M. C., Stewart, E. A., McDannold, N., Quade, B. J., Jolesz, F. A., & Hynynen, K. (2003). MR Imaging– guided Focused Ultrasound Surgery of Uterine Leiomyomas: A Feasibility Study. *Radiology*, *226*, 897–905.

ter Haar, G. (1999). Therapeutic ultrasound. *European Journal of Ultrasound*, *9*(1), 3–9. https://doi.org/10.1016/S0929-8266(99)00013-0

ter Haar, G., & Coussios, C. (2007). High intensity focused ultrasound: Physical principles and devices. *International Journal of Hyperthermia*, *23*(2), 89–104. https://doi.org/10.1080/02656730601186138

Thangavel, K., & Saritaş, E. Ü. (2017). Aqueous paramagnetic solutions for MRI phantoms at 3 T: A detailed study on relaxivities. *Turkish Journal of Electrical Engineering and Computer Sciences*, *25*(3), 2108–2121. https://doi.org/10.3906/elk-1602-123

Thoeny, H. C., De Keyzer, F., Boesch, C., & Hermans, R. (2004). Diffusion-weighted imaging of the parotid gland: Influence of the choice of b-values on the apparent diffusion coefficient value. *Journal of Magnetic Resonance Imaging*, *20*(5), 786–790. https://doi.org/10.1002/jmri.20196

Tietze, A., Mouridsen, K., & Mikkelsen, I. K. (2015). The impact of reliable prebolus T 1 measurements or a fixed T 1 value in the assessment of glioma patients with dynamic contrast enhancing MRI. *Neuroradiology*, *57*(6), 561–572. https://doi.org/10.1007/s00234-015-1502-z

Tofts, P S, & Kermode, A. G. (1989). Blood brain barrier permeability in multiple sclerosis using labelled DTPA with PET, CT and MRI. *Journal of Neurology, Neurosurgery & Psychiatry*, *52*(8), 1019–1020. https://doi.org/10.1136/jnnp.52.8.1019

Tofts, Paul S. (1997). Modeling tracer kinetics in dynamic Gd-DTPA MR imaging. *Journal of Magnetic Resonance Imaging*, *7*(1), 91–101. https://doi.org/10.1002/jmri.1880070113

Tofts, Paul S., Brix, G., Buckley, D. L., Evelhoch, J. L., Henderson, E., Knopp, M. V., Larsson, H. B. W., Lee, T. Y., Mayr, N. A., Parker, G. J. M., Port, R. E., Taylor, J., & Weisskoff, R. M. (1999). Estimating kinetic parameters from dynamic contrast-enhanced T1- weighted MRI of a diffusable tracer: Standardized quantities and symbols. *Journal of Magnetic Resonance Imaging*, *10*(3), 223–232.

Tofts, Paul S., & Parker, G. J. M. (2013). DCE-MRI: Acquisition and analysis techniques. In P. Barker, X. Golay, & G. Zaharchuk (Eds.), *Clinical Perfusion MRI: Techniques and Applications* (pp. 58–74). Cambridge University Press. https://doi.org/10.1017/CBO9781139004053.006

van Osch, M. (2013). Dynamic susceptibility contrast MRI: Acquisition and Analysis Techniques. In P. Barker, X. Golay, & G. Zaharchuk (Eds.), *Clinical Perfusion MRI: Techniques and Applications* (pp. 16–37). Cambridge University Press.

Venkatesan, A. M., Partanen, A., Pulanic, T. K., Dreher, M. R., Fischer, J., Zurawin, R. K., Muthupillai, R., Sokka, S., Nieminen, H. J., Sinaii, N., Merino, M., Wood, B. J., & Stratton, P. (2012). Magnetic resonance imaging-guided volumetric ablation of symptomatic leiomyomata: Correlation of imaging with histology. *Journal of Vascular and Interventional Radiology*, *23*(6), 786-794.e4. https://doi.org/10.1016/j.jvir.2012.02.015

Verpalen, I. M., Anneveldt, K. J., Vos, P. C., Edens, M. A., Heijman, E., Nijholt, I. M., Dijkstra, J. R., Schutte, J. M., Franx, A., Bartels, L. W., Moonen, C. T. W., & Boomsma, M. F. (2020). Use of multiparametric MRI to characterize uterine fibroid tissue types. *Magnetic Resonance Materials in Physics, Biology and Medicine*, *0123456789*. https://doi.org/10.1007/s10334-020-00841-9

Wang, Y., Ren, D., & Wang, W. (2016). The Influence of Oxytocin on the Blood Perfusion of Uterine Fibroids: Contrast-enhanced Ultrasonography Evaluation. *Journal of Medical Ultrasound*, *24*(1), 13–17. https://doi.org/10.1016/j.jmu.2015.11.003

Wei, C., Fang, X., Wang, C. bin, Chen, Y., Xu, X., & Dong, J. ning. (2017). The predictive value of quantitative DCE metrics for immediate therapeutic response of high-intensity focused ultrasound ablation (HIFU) of symptomatic uterine fibroids. *Abdominal Radiology*, 1–7. https://doi.org/10.1007/s00261-017-1426-7

Wei, J.-J., Zhang, X. M., Chiriboga, L., Yee, H., Perle, M. A., & Mittal, K. (2006). Spatial differences in biologic activity of large uterine leiomyomata. *Fertility and Sterility*, *85*(1), 179–187. https://doi.org/10.1016/j.fertnstert.2005.07.1294

Weishaupt, D., Köchli, V. D., & Marincek, B. (2008). *How does MRI work?* (2nd ed.). Springer Berlin Heidelberg. https://doi.org/10.1007/978-3-662-07805-1

Welsch, G. H., Hennig, F. F., Krinner, S., & Trattnig, S. (2014). T2 and T2* Mapping. *Current Radiology Reports*, *2*(8), 1–9. https://doi.org/10.1007/s40134-014-0060-1

Whittall, K. P., MacKay, A. L., Graeb, D. A., Nugent, R. A., Li, D. K. B., & Paty, D. W. (1997). In vivo measurement of T2 distributions and water contents in normal human brain. *Magnetic Resonance in Medicine*, *37*(1), 34–43. https://doi.org/10.1002/mrm.1910370107

Yankeelov, T., & Gore, J. (2009). Dynamic Contrast Enhanced Magnetic Resonance Imaging in Oncology:Theory, Data Acquisition,Analysis, and Examples. *Current Medical Imaging Reviews*, *3*(2), 91–107. https://doi.org/10.2174/157340507780619179

Yoon, S. W., Lee, C., Cha, S. H., Yu, J. S., Na, Y. J., Kim, K. A., Jung, S. G., & Kim, S. J. (2008). Patient selection guidelines in MR-guided focused ultrasound surgery of uterine fibroids: A pictorial guide to relevant findings in screening pelvic MRI. *European Radiology*, *18*(12), 2997–3006. https://doi.org/10.1007/s00330-008-1086-7

Zaher, S., Gedroyc, W. M., & Regan, L. (2009). Patient suitability for magnetic resonance guided focused ultrasound surgery of uterine fibroids. *European Journal of Obstetrics Gynecology and Reproductive Biology*, *143*(2), 98–102. https://doi.org/10.1016/j.ejogrb.2008.12.011

Zhang, L., Zhang, W., Orsi, F., Chen, W., & Wang, Z. (2015). Ultrasound-guided high intensity focused ultrasound for the treatment of gynaecological diseases: A review of safety and efficacy. *International Journal of Hyperthermia*, *00*(00), 1–5. https://doi.org/10.3109/02656736.2014.996790

Zhu, Y., Keserci, B., Viitala, A., Wei, J., Yang, X., & Wang, X. (2016). Volumetric MR-guided high-intensity focused ultrasound ablation to treat uterine fibroids through the abdominal scars using scar patch: A case report. *Journal of Therapeutic Ultrasound*, *4*(1), 1–6. https://doi.org/10.1186/s40349-016-0064-9

Zowall, H., Cairns, J. A., Brewer, C., Lamping, D. L., Gedroyc, W. M. W., & Regan, L. (2008). Cost-effectiveness of magnetic resonance-guided focused ultrasound surgery for treatment of uterine fibroids. *BJOG: An International Journal of Obstetrics and Gynaecology*, *115*(5), 653–662. https://doi.org/10.1111/j.1471-0528.2007.01657.x

TURUN
YLIOPISTO
UNIVERSITY
OF TURKU

Painosalama, Turku, Finland 2021

ISBN 978-951-29-8692-7 (PRINT)
ISBN 978-951-29-8693-4 (PDF)
ISSN 0355-9483 (Print)
ISSN 2343-3213 (Online)